127

LA-3915

AUTHOR'S COPY

LOS ALAMOS SCIENTIFIC LABORATORY
of the
University of California
LOS ALAMOS • NEW MEXICO

Shock Wave Compression of Benzene, Carbon Disulfide, Carbon Tetrachloride, and Liquid Nitrogen

UNITED STATES
ATOMIC ENERGY COMMISSION
CONTRACT W-7405-ENG. 36

Printed in the United States of America. Available from Clearinghouse for Federal Scientific and Technical Information National Bureau of Standards, U. S. Department of Commerce Springfield, Virginia 22151

Price: Printed Copy $3.00; Microfiche $0.65

LA-3915
UC-34, PHYSICS
TID-4500

LOS ALAMOS SCIENTIFIC LABORATORY
of the
University of California
LOS ALAMOS • NEW MEXICO

Report written: April 1968

Report distributed: April 30, 1968

Shock Wave Compression of Benzene, Carbon Disulfide, Carbon Tetrachloride, and Liquid Nitrogen*

by

Richard Dean Dick

*Also submitted as a dissertation in partial fulfillment of the requirements for the degree of Doctor of Philosophy in Physics from Arizona State University.

ABSTRACT

Shock waves generated by high explosives were used to obtain Hugoniot data for benzene, carbon disulfide, and carbon tetrachloride initially at 300°K and liquid nitrogen initially at 75°K. Electrical pin contactors were used to determine the shock velocity in a dural standard plate and in the liquids. From these data and the known dural equation of state, the Hugoniot curves for the liquids were determined by means of the conservation relations and continuity conditions. Dynamic pressures achieved ranged from 20 to 600 kbar in the samples. A plot of the shock velocity (U_s) versus particle velocity (U_p) data for benzene reveals three regions each of which is described by a linear relationship. This is indicative of a transition occurring at 125 kbar and ending at 180 kbar. The carbon disulfide U_s-U_p plot reveals a lower region fitted by a straight line, a middle region of constant shock velocity, and a upper region fitted by another straight line. The middle portion corresponds to 64 kbar and the liquid is believed to transform at this pressure to the so-called black form of carbon disulfide. Two straight lines with differing slopes describe the U_s-U_p data of carbon tetrachloride. This may be the result of crossing a fusion line. The liquid nitrogen U_s-U_p plot is interpreted to have four possible regions and are (1) a lower portion fitting a straight line, (2) a region of constant shock velocity, (3) a region which fits a straight line of steep slope, and (4) the highest region fitting another straight line.

This behavior is hypothesized to be the result of the Hugoniot crossing phase lines in the vicinity of a triple point.

Although carbon disulfide and carbon tetrachloride are normally insulators, both become electrically conductive at pressures near 70 kbar.

Some thermodynamic quantities such as temperatures on the Hugoniot, isentropes, and isotherms were calculated using a computer program fashioned with a thermodynamic description based on the Mie-Gruneisen form for the equation of state.

ACKNOWLEDGEMENTS

The experimental program leading to this dissertation could not have been accomplished without the support of the Los Alamos Scientific Laboratory and especially from many people in the GMX Division. I am very appreciative of the sanctioning provided by Dr. Duncan P. MacDougall, the GMX Division Leader. I am deeply grateful to Dr. Eric L. Peterson, GMX-4 Group Leader, for allowing me to carry out the research in Group GMX-4 and for his continual interest in the program. I wish to thank Dr. William E. Deal for serving as my dissertation advisor at this laboratory in addition to giving moral support. This research would have been much more difficult were it not for Thomas E. Gould providing the technical talent necessary to build and fire the experimental assemblies. I also thank Richard H. Warnes and John Skalyo, Jr. for fruitful discussions and valuable assistance throughout this study.

TABLE OF CONTENTS

LIST OF TABLES

LIST OF FIGURES

FIGURE PAGE

I. INTRODUCTION

A. Purpose

A study was made to determine some of the properties of benzene (C_6H_6), carbon disulfide (CS_2), and carbon tetrachloride (CCl_4) at ambient temperatures and liquid nitrogen (LN_2) at 75°K when compressed by dynamic pressures to several hundred thousand atmospheres. The dynamic pressures are achieved by plane shock waves generated from high explosives propagating through the liquids. The program required the development of experimental techniques and apparatus compatible with the instrumentation available in Group GMX-4 of the Los Alamos Scientific Laboratory. The investigation includes the gathering of pressure-volume data, examination of the phase transitions, a very brief search for electrical conduction in the compressed state, and calculation of some related thermodynamic quantities such as temperature on the Hugoniot.

B. Previous Investigations

The original compression work on liquids was performed in the seventeenth and eighteenth centuries by John Canton,[1] Jacob Perkins,[2] L. Cailleter,[3] E. H. Amagat,[4] and others employing hydrostatic pressure techniques; the main interest being the phenomenon of volume change. Amagat, using special sealing methods, was able to attain pressures of nearly 3000 atmospheres in the liquids.

From the close of the nineteenth century to the early part of the twentieth century, G. Tammann[5] and T. W. Richards[6] investigated the effects of pressure on solutions, organic liquids, and some elements. Their efforts were noteworthy because of their extensive and systematic experimentation on so many materials. Tammann attained pressures of about 3 kbar (1 kbar = 10^9 dynes/cm^2 or 986.9 atmospheres) and Richards, 500 bar.

P. W. Bridgman[7-13] at Harvard University, starting about 1910 and continuing for nearly 50 years, contributed enormously to the static high pressure field. He developed new apparatus and techniques to study a large number of substances including liquids in this investigation. Bridgman obtained compression data, fusion curves, latent heats of fusion, entropy changes upon freezing, and other thermodynamic quantities. The pressure range covered in these liquids was from one atmosphere to about 10 kbar.

The first dynamic pressure data on organic liquids and water was published by J. M. Walsh and M. H. Rice[14, 15] from experiments performed at the Los Alamos Scientific Laboratory. Using optical techniques, they determined the pressure and associated volume change and observed opacity changes in some of the liquids under shock conditions. They made a very thorough study of water to pressures of 450 kbar but their coverage of the organic liquids was very limited. The pressure range covered in this study is from about 20 to 600 kbar.

More extensive data on these liquids and others were gathered by M. A. Cook and L. A. Rogers[16] at the University of Utah using optical methods. They covered a pressure range of 4-130 kbar

with the main interest in measuring the compressibility from which they calculated the internal pressure and cohesive energy density.

The shock compression of liquid nitrogen was reported by V. N. Zuborev and G. S. Telegin[17] using experimental techniques quite similar to those of this investigation. They attained pressures in liquid nitrogen of 30-300 kbar and used the data to compare with a modified Lennard-Jones and Devonshire intermolecular potential.

At the present time, shock compression studies are also being conducted on liquids at the Lawrence Radiation Laboratory at Livermore, California, with the basic interest in condensed noble gases.[18]

II. THEORY OF SHOCK WAVES

A. Introduction

A shock front is characterized by a very rapid change in mechanical properties and thermodynamic state of a material produced by a violent disturbance. This disturbance in the present investigation is derived from the detonation of high explosives. The theory presented in succeeding sections is confined to the propagation of a single shock wave in materials for which the sound speed increases with pressure beyond some initial linear portion; that is the compressibility of the medium decreases as the pressure increases. Most materials possess this property, including the four liquids studied in this investigation.

The formation of a shock front can be pictured qualitatively by the following model. A piston is accelerated into a medium and this motion is considered divided into a large number of small successive movements. The initial motion causes a small disturbance to propagate into the medium at the sound speed. The material is compressed behind this disturbance resulting in an increase in the sound speed. The next disturbance will then propagate at a slightly higher sonic velocity than the previous one. The faster wave tends to overtake and unite with the slower wave. After many of these disturbances have been generated and propagated in the compressed medium, they collect at a single discontinuity forming a shock front. This front travels at a velocity between the sound speed of the undisturbed

material and the compressed material behind the shock.

The discontinuity or shock front under actual conditions acquires a very large but finite slope due to the presence of viscosity and heat conduction. In most situations, treating the shock front as a discontinuity seems to be adequate in terms of present experimental techniques.

The basic properties of the state of the medium across a shock front will be presented briefly. A more detailed treatment can be found in references 19 and 20. First, the entropy of the material increases across the shock front and the increase is third order in the shock strength (that is $P-P_0$, V_0-V, or $\rho-\rho_0$). The pressure, density, and energy increase very abruptly in going to the compressed state and these changes differ from isentropic changes by third order in the shock strength. Shocks are compressive, meaning the pressure and density increase as the materials are compressed. Lastly, the shock wave velocity is supersonic with respect to the unshocked material and subsonic with respect to the material behind the shock front. The shock process is assumed to be adiabatic since the time scale is much too short to allow appreciable heat transfer.

B. Conservation Relations for a Shock Wave

The derivation of the Rankine-Hugoniot equations or the conservation relations[21, 22, 23] is begun by considering a plane uniform shock front traveling into a medium which behaves in a manner described in Section A. The assumptions in the derivation are (1) steady state conditions exist behind the shock front; that is, no physical quantities vary with time, (2) the compressed material is in thermodynamic equilibrium behind the shock front, (3) the pressure

wave is the means by which energy and momentum are transferred, (4) the momentum and energy are transported by contact forces, (5) behind the shock front, hydrostatic conditions exist, and (6) the material acts as a fluid. The steady state condition probably does not exist within the shock front but the final state attained is not affected appreciably by structure in the shock front. Steady state is essential, however, in deriving the conservation relations and thermodynamic equilibrium is necessary for a meaningful description of the compressed material.

Consider the one- dimensional shock wave illustrated in Fig. 1 in which an observer is attached to a coordinate system moving with the shock front. The region of interest is ahead and behind the discontinuity as illustrated by lines marked A and B. In the figure, U_s is the velocity of the shock wave, U_p is the velocity each mass element receives after passing through the shock front (neglecting thermal motion), E is the specific internal energy, P is the pressure, and ρ is the density of the material behind the shock wave. The subscripted variables E_0, P_0, and ρ_0 represent the undisturbed material ahead of the shock wave. The undisturbed material with a density ρ_0 is flowing into the discontinuity with a velocity U_s and flows out with a velocity $U_s - U_p$ and a density ρ. Hence, the mass flowing in during time δt is $\rho_0(U_s - U_{p0})\delta t$ and mass flowing out is $\rho(U_s - U_p)\delta t$. Since there are no sources or sinks, the mass must be conserved across the shock front. Then

$$\rho_0(U_s - U_{p0}) = \rho(U_s - U_p). \tag{1}$$

Equation (1) can be written in terms of specific volume V_0 and V in the form

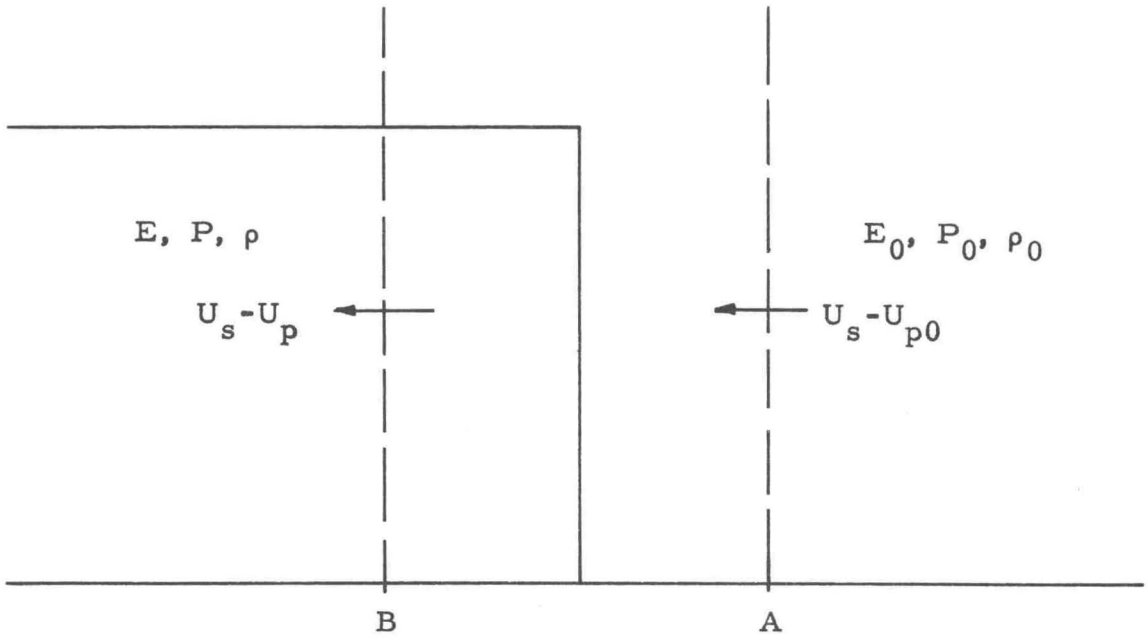

Fig. 1. Diagram of a one-dimensional shock wave.

$$V/V_0 = (U_s - U_p)/(U_s - U_{p0}) \tag{2}$$

where

$$V = 1/\rho \text{ and } V_0 = 1/\rho_0.$$

The mass flowing into the shock front has momentum $\rho_0(U_s - U_{p0})\delta t(U_s - U_{p0})$ and flows out with momentum $\rho(U_s - U_p)\delta t(U_s - U_p)$. The change in momentum per unit time is the difference between these two quantities and must equal the net force exerted per unit area across the shock front. This net force per unit area normal to the shock front is the pressure difference $P - P_0$. Hence,

$$P - P_0 = \rho_0(U_s - U_{p0})^2 - \rho(U_s - U_p)^2 \tag{3}$$

where P_0 is pressure ahead of the shock front and P is the pressure behind. Replacing ρ from Eq. (1), the conservation of momentum statement becomes in a more familiar and usable form

$$P - P_0 = \rho_0(U_s - U_{p0})(U_p - U_{p0}). \tag{4}$$

The conservation of energy across the shock front may be expressed by equating the network done per unit area per unit time by the pressure forces to the change in kinetic and internal energy of a mass element. The work done at A (see Fig. 1) is $P_0U_{p0}\delta t$ and at B the work required to bring a mass element to a velocity U_p in time δt is $PU_p\delta t$. Hence, the net work done is $(PU_p-P_0U_{p0})\delta t$. The increase in kinetic energy across the shock is $\rho_0(U_s-U_{p0})\delta t(U_p^2-U_{p0}^2)/2$ and in the internal energy is $\rho(U_s-U_{p0})\delta t(E-E_0)$. Equating the net work done to the increase in specific energy,

$$PU_p-P_0U_{p0} = \rho_0(U_s-U_{p0})\left[(U_p-U_{p0})^2 + (E-E_0)\right]/2. \qquad (5)$$

The velocities in Eq. (5) can be eliminated by using Eqs. (1) and (4) to obtain the more usual form for the Hugoniot equation

$$E-E_0 = (P+P_0)(V_0-V)/2. \qquad (6)$$

If the material ahead of an advancing shock wave is stationary, then U_{p0} is zero; also in a single shock process, P_0 represents atmospheric pressure and can be neglected since this pressure is very much less than the dynamic pressures available from explosives. The conservation relations become with these simplifications

$$V/V_0 = (U_s-U_p)/U_s \qquad (7)$$

$$P = \rho_0U_sU_p \qquad (8)$$

$$E-E_0 = P(V_0-V)/2. \qquad (9)$$

All the quantities P, V, E, U_s, and U_p are defined for a given steady state shock front and the locus of any pair refers to a Hugoniot curve in the corresponding space.

C. Stability of Shock Waves

The behavior of most materials subjected to shock conditions will satisfy the so-called Bethe-Weyl conditions.[19] They are

$$(\partial P/\partial V)_S < 0 \tag{10}$$

$$(\partial^2 P/\partial V^2)_S > 0 \tag{11}$$

$$(\partial P/\partial S)_V > 0. \tag{12}$$

The first two conditions state the requirement that the shock velocity increase with pressure and the last condition states that the shock process is not isentropic; however, the shock process is assumed to be adiabatic. These are the necessary requisites for a shock wave to be stable, meaning, the wave will not separate into multiple waves nor exhibit dispersion. Dispersion would result if the Hugoniot curve in the P-V plane were concave downward.

There are two general properties of materials for which the second Bethe-Weyl condition is sometimes not satisfied, namely, elastic-plastic effects and phase changes. Because liquids have negligible rigidity, elastic-plastic effects are not observed and hence will not be discussed. Phase changes do occur in liquids and their effects will be discussed in terms of shock wave stability.

Consider the Hugoniot curve of Fig. 2 (a) in which a phase change occurs at P_1, V_1. A shock wave which connects the state P_0, V_0 to any other state on the Hugoniot curve up to P_1, V_1 will be stable since the shock velocity increases with the pressure. The conservation relations expressed in Eqs. (7), (8), and (9) can be rearranged to provide an expression for the shock velocity in terms

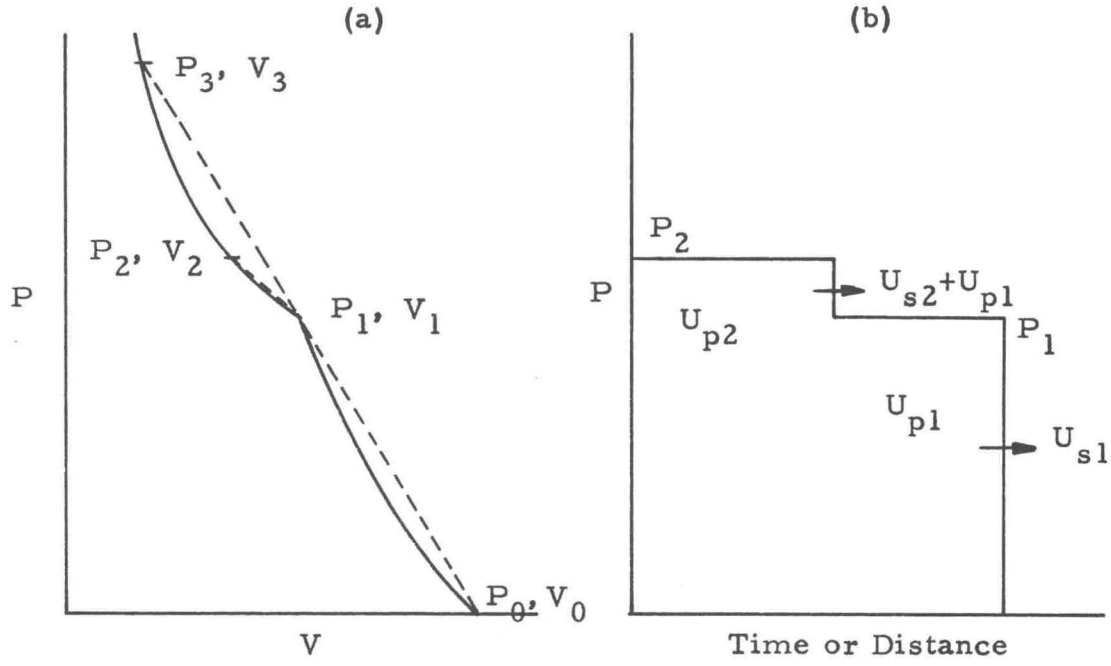

Fig. 2 P-V diagram for a material that undergoes a phase transition and the resulting pressure profile.

of pressure and volume in the form

$$U_s = V_0\sqrt{\frac{P-P_0}{V_0-V_1}} = V_0\sqrt{-\frac{\Delta P}{\Delta V}}\,.$$

The shock velocity is then proportional to the square root of the slope of line $(-\Delta P/\Delta V)$, called the Rayleigh line, which connects the initial and final states. When going to the state P_2, V_2 from the initial state, the slope of the line joining them is less than the slope of the ray connecting the original state to P_1, V_1. Thus, the velocity of the shock wave has decreased with pressure constituting an unstable condition. In this circumstance, two stable shock waves are formed; the first has the characteristics of the onset of the transition at P_1, V_1 and the second is associated with going from the state P_1, V_1 to P_2, V_2. The shock wave that accompanies the transition travels faster than the second wave and as a result separation between these two waves increases in time and space when traversing

the sample. This situation is depicted in Fig. 2(b).

Referring again to Fig. 2, the first wave corresponding to the state P_2, V_2 travels at U_{s1} with respect to the material ahead and $U_{s1} - U_{p1}$ with respect to the material behind it. The second wave travels at U_{s2} with respect to the material ahead (state P_1, V_1). The shock wave is unstable when $U_{s2} < U_{s1} - U_{p1}$ and from Eqs. (7) and (8) can be rewritten as

$$U_{s1} - U_{p1} = V_1\sqrt{\frac{P_1 - P_0}{V_0 - V_1}} \tag{13}$$

and

$$U_{s2} = V_1\sqrt{\frac{P_2 - P_1}{V_1 - V_2}} \ . \tag{14}$$

Since

$$U_{s2} < U_{s1} - U_{p1} \tag{15}$$

then upon substitution of Eqs. (13) and (14) into (15)

$$\frac{P_2 - P_1}{V_1 - V_2} < \frac{P_1 - P_0}{V_0 - V_1} \ . \tag{16}$$

This then is the condition for a shock wave to separate into two stable shock waves at the state P_1, V_1. If $U_{s2} \geq U_{s1} - U_{p1}$ the shock wave cannot break up and is considered stable.

The stability question arises when the Hugoniot curve crosses a phase boundary. Consider the P-V diagram in Fig. 3 which represents one of many possible phase transition models. Here the two phase boundaries are represented by A and B and between them is a mixed-phase region. The coordinate P_1, V_1 represents the position at which the material begins to transform from phase A to B. For shock strengths less than P_1, the final

state remains in phase A where the shock wave is stable. Once the shock strength exceeds this point, the shock wave becomes unstable and two waves are formed. The first wave has the characteristics of the phase transition pressure and the second wave represents the remainder of the input pressure. The shock profile, after allowing the two waves to separate, will have the features illustrated in Fig. 2(b). Beyond P_2, V_2, the material is completely transformed to phase B and the shock wave is stable once again.

Measurement of the free surface velocity of solids, after the shock wave has traversed the sample, serves to detect a phase transition and establish the transition pressure, if there is sufficient separation of the two waves. Liquids, however, do not lend themselves readily to this type of measurement; so a different technique is necessary.

Once the presence of the two-wave structure is established, the more difficult question remains as to the cause of the

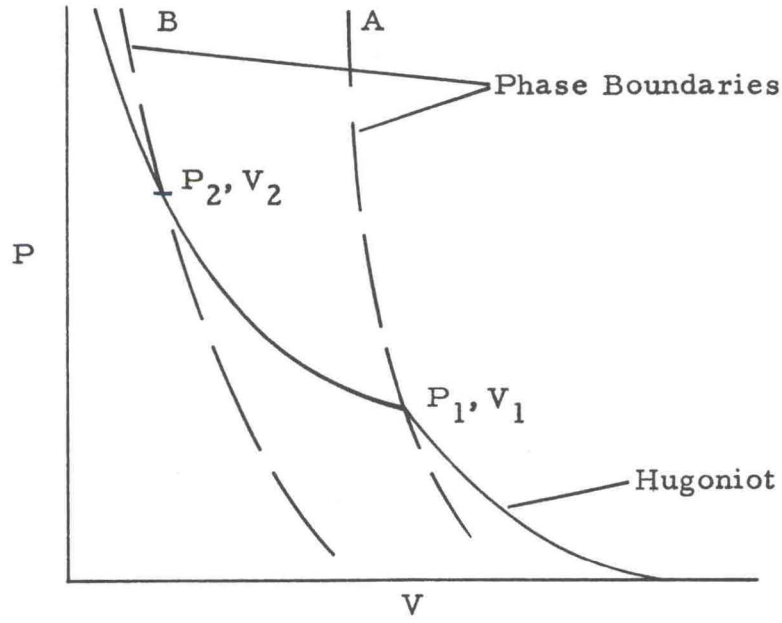

Fig. 3 Influence of phase boundaries on a P-V Hugoniot.

transition. The usual explanation for the two-wave structure in solids is a solid-solid transition[24, 25] in which the material transforms from one crystal structure to another. A two-wave structure in liquids is not easily explained, however. Usually a liquid-solid transition or vice versa does not produce a large enough change in volume and consequently the two-wave structure may not be observable. The transition may be due to a sudden change in the number of nearest neighbors, polymerization upon compression, or the solidification of the liquid as the pressure is applied and then a solid-solid transition occurring.

D. Interaction of a Shock Wave with an Interface

The collision of a shock wave with an interface between two media has not only theoretical importance, but important experimental application. The basis for describing this interaction is that the particle velocity and pressure are continuous across the interface and the conservation relations are valid. Consider the case in which a plane shock wave collides at normal incidence with an interface between two media. Fig. 4 illustrates the situation before and after collision for two cases involving differing media. The expressions relating the pressures and particle velocities for the two media will be derived in a form such that the left-going wave can be either a reflected shock or a rarefaction wave. The relative impedances (initial density times the shock velocity) determines which condition prevails. Application of continuity across the interface yields

$$P_2 = P_3 \tag{17}$$

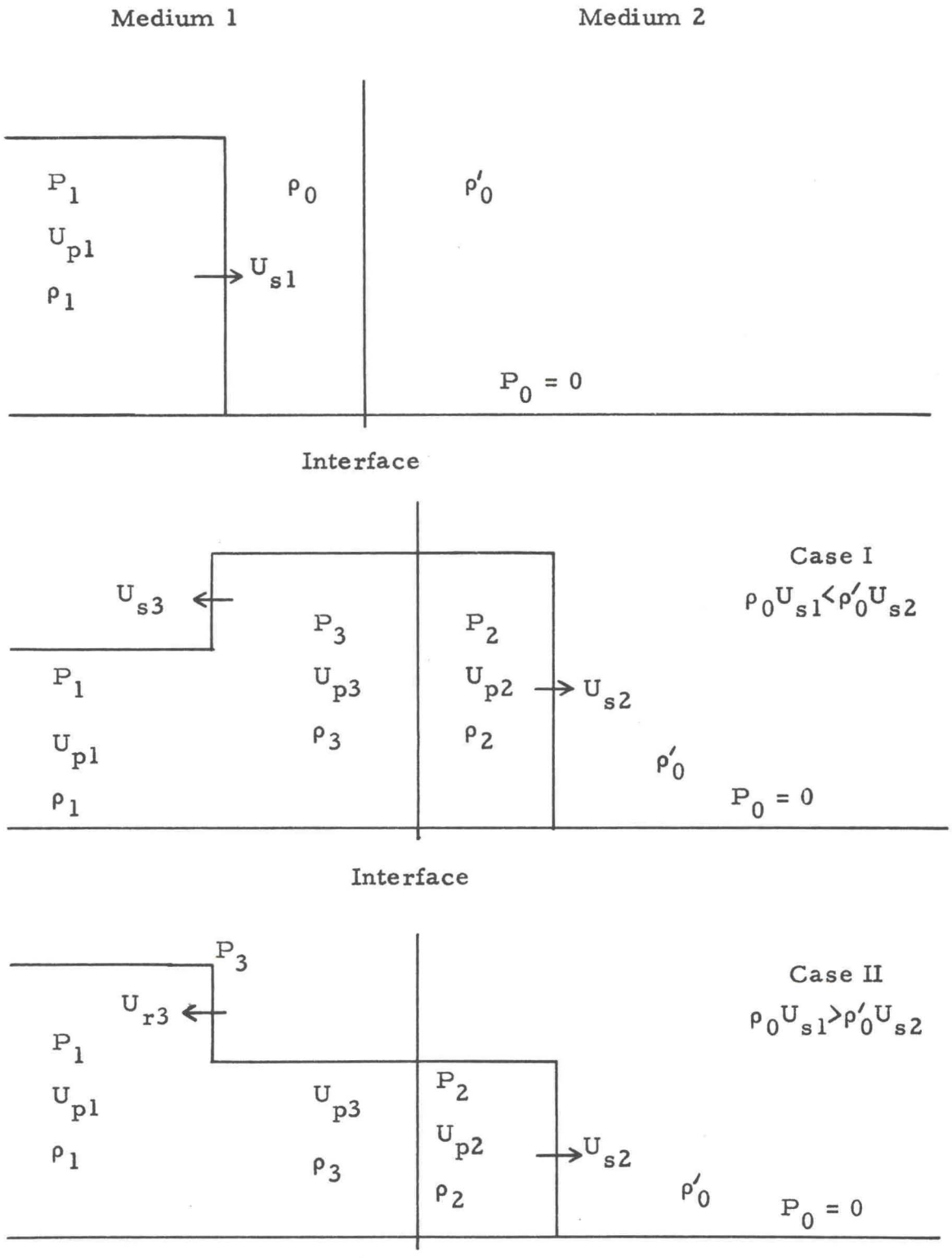

Fig. 4. Interaction of a shock wave with an interface involving differing impedances.

$$U_{p2} = U_{p3}. \tag{18}$$

From Eq. (4)

$$P_1-P_0 = \rho_0(U_{s1}-U_{p0})(U_{p1}-U_{p0}),$$

$$P_2-P_0 = \rho'_0(U_{s2}-U_{p0})(U_{p2}-U_{p0}),$$

$$P_3-P_1 = \rho_1(U_{s3}-U_{p1})(U_{p3}-U_{p1}).$$

The material ahead of the shock waves U_{s1} and U_{s2} is assumed at rest so that $P_0 = U_{p0} = 0$. Using the continuity conditions and the first and third of the above equations,

$$P_2 = \rho_0 U_{s1} U_{p1} + \rho_1(U_{s3}-U_{p1})(U_{p2}-U_{p1}).$$

Substituting for P_2 and simplifying

$$\frac{U_{p2}}{U_{p1}} = \frac{\rho_0 U_{s1}-\rho_1(U_{s3}-U_{p1})}{\rho'_0 U_{s2}-\rho_1(U_{s3}-U_{p1})} \tag{19}$$

and

$$\frac{P_2}{P_1} = \frac{\rho'_0 U_{s2}\left[\rho_0 U_{s1}-\rho_1(U_{s3}-U_{p1})\right]}{\rho_0 U_{s3}\left[\rho'_0 U_{s2}-\rho_1(U_{s3}-U_{p1})\right]}. \tag{20}$$

The shock waves moving to the right, such as U_{s1} and U_{s2} are defined as traveling in the positive direction and those to the left, such as U_{s3} are moving in the negative direction. In an experiment, the impedances $\rho_0 U_{s1}$ and $\rho'_0 U_{s2}$ for the media are readily determined from the measured shock velocities. However, the quantity $\rho_1 U_{s3}$ is very troublesome due to the difficulty in measuring U_{s3} by the technique used here. This problem can be overcome if an extension of the acoustic approximation[19] is used to write

$$\rho_0 U_{s1} = -\rho_1(U_{s3}-U_{p1}). \tag{21}$$

Equations (19) and (20) can then be simplified to read

$$\frac{U_{p2}}{U_{p1}} = \frac{2\rho_0 U_{s1}}{\rho_0 U_{s1} + \rho'_0 U_{s2}} \tag{22}$$

and

$$\frac{P_2}{P_1} = \frac{2\rho'_0 U_{s2}}{\rho_0 U_{s1} + \rho'_0 U_{s2}} . \tag{23}$$

The expressions for the ratio between the two mass velocities and between the two pressures were derived without stating which medium had the larger impedance. Whether the wave reflected back into medium 1 is a reflected shock wave or a rarefaction wave depends upon the relative magnitudes of the impedances. If medium 1 has a smaller impedance than medium 2, the wave sent back into the compressed state of medium 1 will be a reflected shock wave. Conversely, a rarefaction wave is reflected back into medium 1 when medium 1 has the larger impedance. A shock wave is transmitted into medium 2 regardless of the impedances. The pressure profiles for these two cases are illustrated in Fig. 4. Equations (22) and (23) can be used to calculate the approximate values of mass velocity and pressure in medium 2 if, along with the shock velocity measurements, the pressure in medium 1 is known. Case II of Fig. 4 represents the present experimental arrangement in which medium 1 is aluminum and medium 2 is the liquid.

E. Impedance Matching

An alternative and more useful approach to the preceding analysis can be developed if the interaction of a shock wave with an interface is examined in the pressure versus particle velocity plane. The curve in this plane starting from the origin represents the locus

of all P-U_p states in a medium which can be achieved by a right-going shock wave. Consider the Hugoniot curves for two media in Fig. 5. Case II of Fig. 4 illustrates the pressure profile for this situation. The sequence of events can be described in the following manner. Medium 1 is brought from the initial state P = 0, $U_p = 0$ to the state P_1, U_{p1} by the action of a right-going shock wave S_1. When the shock wave interacts with the interface between the two media, a transmitted shock wave S_2 transforms medium 2 to the state P_2, U_{p2} from the initial state. At the same time, a rarefaction wave S_3 is reflected back into medium 1 causing the material to be relieved to the state P_2, U_{p2}. This state is represented by the intersection of the rarefaction curve which corresponds to the locus of P, U_p states attained behind the rarefaction wave in medium 1 and the Hugoniot curve for medium 2. This intersection point must necessarily be the point at which the continuity conditions are satisfied. The rarefaction curve is actually a release isentrope and for most solids there is little difference between a mirror image of the Hugoniot curve and this isentrope. Another observation concerning the shock wave-interface interaction is that the straight lines which connect the origin and the points P_1, U_{p1} and P_2, U_{p2} have slopes of $\rho_0 U_{s1}$ and $\rho'_0 U_{s2}$ respectively and are the quantities normally measured in an experiment. This leads to the impedance-match technique or graphical solution method for determining the pressure and particle velocity in an unknown material, when interfaced with a known material.

The application of this technique, illustrated in Fig. 6, utilizes 2024 aluminum alloy as the known standard material in

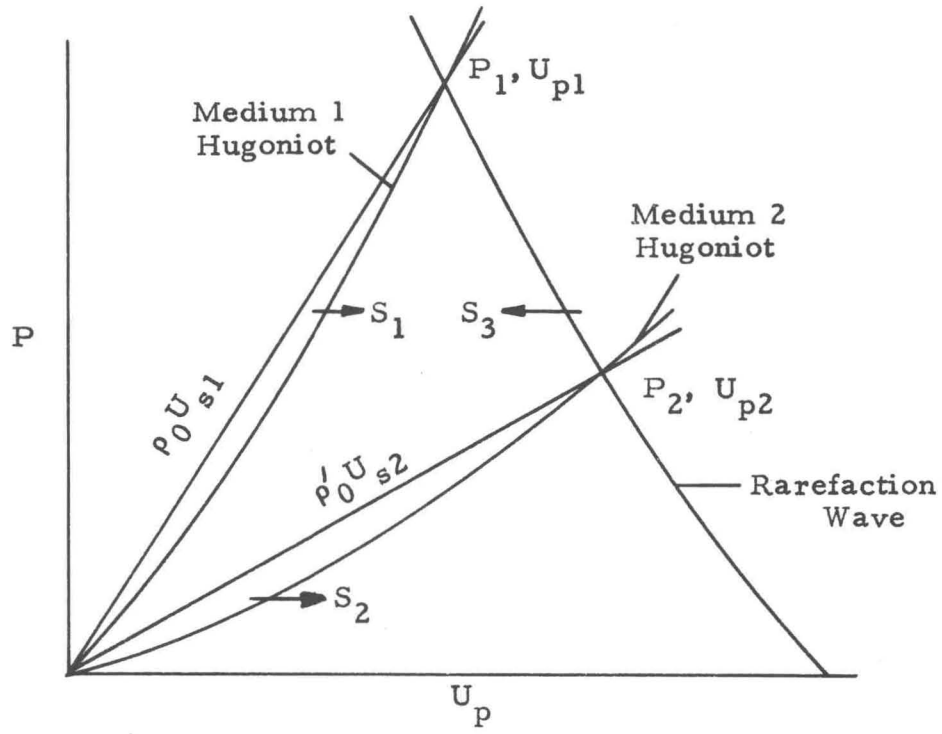

Fig. 5. Interaction of a shock wave with a medium of lower impedance.

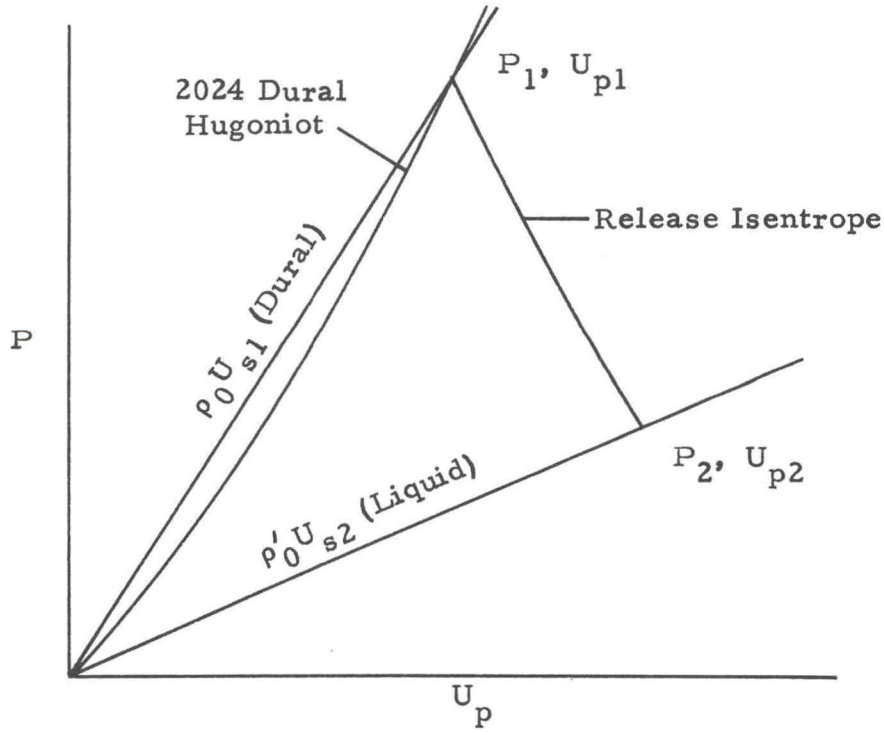

Fig. 6. Graphic representation of the impedance-match method.

contact with the liquid samples. This particular aluminum alloy was chosen because the Hugoniot curve has been measured more extensively than any other solid.[26] The procedure is to measure the shock velocity in the aluminum standard and in the liquid samples. Then the state P_1, U_{p1} for the 2024 dural is identified from the intersection of the line of slope $\rho_0 U_{s1}$ with its Hugoniot curve. The release isentrope which is calculated from this measured state is constructed and the intersection point of this curve with the ray of slope $\rho'_0 U_{s2}$ yields the compressed state P_2, U_{p2} for the sample. This method was used to determine the Hugoniot curves for the liquids studied here.

F. Thermodynamics of the Shocked State

Through the Hugoniot relation and the conservation of mass and momentum, the measured quantities U_s, U_p, and ρ_0 are connected with changes in internal energy in terms of the mechanical variables P and V. It is then possible to calculate the temperature and the local sound speed on the Hugoniot and, with the aid of simple assumptions, to determine isentropes and isotherms off the Hugoniot.

These calculations are based on the Mie-Gruneisen equation of state[21, 27] for solids and is written in the form

$$\Gamma/V = (P-P_0) / (E-E_0) \qquad (24)$$

where V is the volume, P is the pressure, E is the energy, and Γ is the Gruneisen ratio and assumed to be a function only of volume. The zero subscript refers to a reference state.

The Gruneisen ratio can be written in terms of other thermodynamic quantities. By differentiating Eq. (24) with respect

to E at constant V

$$\Gamma/V = (\partial P/\partial E)_V \tag{25}$$

or

$$\Gamma = -\frac{V}{C_P}\left(\frac{\partial P}{\partial V}\right)_S\left(\frac{\partial V}{\partial T}\right)_P . \tag{26}$$

The bulk modulus at constant entropy is defined by

$$B_S = -V(\partial P/\partial V)_S \tag{27}$$

and the volume expansion coefficient by

$$\beta = (1/V)(\partial V/\partial T)_P . \tag{28}$$

Then Eq. (26) becomes

$$\Gamma = B_S\beta/\rho C_P . \tag{29}$$

Thus Γ at atmospheric pressure and low temperature can be determined from experimental data for the density, specific heat, bulk modulus, and thermal expansion coefficient.

The Mie-Gruneisen equation of state used with the approximation that

$$\rho\Gamma = \rho_0\Gamma_0 \tag{30}$$

where Γ_0 is the thermodynamic value determined from Eq. (24) and ρ_0 is the initial density, provides a reasonable model for many solids subjected to shock compression.[21, 28] Due to this simplifying assumption facility is gained in calculating some thermodynamic properties off the Hugoniot and so this form for equation of state was adopted for the liquids studied. The model is probably inadequate for liquids because the theory was originally developed for solids. Other reasons for suggesting the model inadequate are the large compressibilities which give rise to high temperatures and changes in the specific heat at these elevated temperatures, but the method does provide a starting place for making calculations.

One of the facts that has been discovered from single shock measurements on many solids and liquids is that over the pressure range accessible with plane explosive systems the shock velocity U_s and particle velocity U_p exhibit a linear relationship of the form

$$U_s = C + MU_p \ . \tag{31}$$

A particular relationship only holds within a given phase. The theoretical significance of this linear relationship has been investigated[29, 30] to some extent but at the present is still not well understood. By combining Eq. (31) with Eqs. (7) and (8), the Hugoniot pressure P_H can be written in terms of the corresponding volume V as

$$P_H = \frac{C^2(V_0-V)}{\left[V_0-M(V_0-V)\right]^2} \ . \tag{32}$$

Isentropes and isotherms can be calculated from the Mie-Gruneisen equation of state as expressed in Eq. (24) when the pressure P and the specific energy E are related to the corresponding quantities on the Hugoniot curve H as a function of volume. Assuming Γ/V is constant, for an isentrope Eq. (24) becomes

$$P_S - P_H = k(E_S - E_H) \ , \tag{33}$$

where P_S and E_S are the pressure and energy on an isentrope and

$$k = \Gamma/V = \Gamma_0/V_0 \ . \tag{34}$$

If Eq. (33) is differentiated with respect to V, the result is a differential equation for pressure along an isentrope

$$\left(\frac{\partial P}{\partial V}\right)_S - \left(\frac{\partial P}{\partial V}\right)_H = k\left(\frac{\partial E}{\partial V}\right)_S - \left(\frac{\partial E}{\partial V}\right)_H \ . \tag{35}$$

Since P and E are functions of volume on a given isentrope then

$$\left(\frac{\partial P}{\partial V}\right)_S = \frac{dP_S}{dV} \ , \ \left(\frac{\partial P}{\partial V}\right)_H = \frac{dP_H}{dV}$$

$$\left(\frac{\partial E}{\partial V}\right)_H = \frac{dE_H}{dV} \ , \ \left(\frac{\partial E}{\partial V}\right)_S = \frac{dE_S}{dV} = -P_S \ . \tag{36}$$

Equation (35) then simplifies to

$$\frac{dP_S}{dV} + kP_S = \frac{d}{dV}(P_H - kE_H) \ . \tag{37}$$

The pressure and energy on the Hugoniot are expressed as

$$P_H = \frac{C^2 a}{(V_0 - Ma)^2}$$

$$E_H = P_H a/2$$

when $a = V_0 - V$ is substituted into Eqs. (6) and (32). Substitution of derivatives of P_H and E_H with respect to a into Eq. (37) yields

$$\frac{dP_S}{da} - kP_S = \frac{C^2}{(V_0 - Ma)^3}\left[V_0 + a(M - kV_0)\right] . \tag{38}$$

This first order differential equation can be solved using the integrating factor $\exp(\int k\,da)$. Hence,

$$P_S = Ae^{ka} + e^{ka}\int e^{-ka} C^2 \left[\frac{V_0 + a(M - kV_0)}{(V_0 - Ma)^3}\right] da \tag{39}$$

where A is a constant of integration. The integral term can be performed in a never ending series of integrations by parts, but an easier method using information gained from integrating by parts is to assume a series solution of the form

$$P_S = Ae^{ka} + \frac{C^2}{(V_0 - Ma)^2} \sum_{i=0}^{\infty} A_i a^i \ . \tag{40}$$

The A_i's must be chosen such that Eq. (38) is satisfied for all powers of a. The recursion relation for the A_i's which satisfies this requirement is

$$A_{i+1} = -\frac{(2M-kV_0-iM)A_i+kMA_{i-1}}{(i+1)V_0} \quad \text{for } i \geq 2 \ . \tag{41}$$

Integration by parts suggests that

$$A_0 = 0,\ A_1 = 1,\ A_2 = 0, \text{ and } A_3 = -kM/3V_0 \ . \tag{42}$$

Expanding Eq. (40) to obtain the first three terms and using the results from Eqs. (32) and (42), the solution becomes

$$P_S = P_H + Ae^{k\alpha} + \frac{C^2}{(V_0-M\alpha)^2} \sum_{i=3}^{\infty} A_i \alpha^i \ . \tag{43}$$

The constant of integration A is determined from the point at which the Hugoniot and the isentrope curves cross. Here $P_S = P_H$ and $\alpha = \alpha_H$ so that

$$P_H = P_H + Ae^{k\alpha_H} + \frac{C^2}{(V_0-M\alpha_H)^2} \sum_{i=3}^{\infty} A_i \alpha_H^i$$

and

$$A = -\frac{C^2 e^{-k\alpha_H}}{(V_0-M\alpha_H)^2} \sum_{i=3}^{\infty} A_i \alpha_H^i \ . \tag{44}$$

From Eq. (43), the pressure in terms of α anywhere along an isentrope can be calculated since the A_i's are determined from Eq. (41), A is found from Eq. (44), and P_H and α_H are experimentally determined values.

The calculation of an isotherm is very similar. Starting again with Eq. (24)

$$P_T - P_H = \Gamma/V(E_T - E_H) \tag{45}$$

where P_T and E_T are the pressure and energy along an isotherm. Differentiating Eq. (45) with respect to volume yields

$$\left(\frac{\partial P}{\partial V}\right)_T - k\left(\frac{\partial E}{\partial V}\right)_T = \left(\frac{\partial P}{\partial V}\right)_H - k\left(\frac{\partial E}{\partial V}\right)_H \tag{46}$$

which represents the differential equation for pressure along an isotherm. At this point, it becomes advantageous to express $(\partial E/\partial V)_T$

in terms of the pressure and known thermodynamic quantities. If entropy and energy are considered functions of T and V, then

$$dS = \left(\frac{\partial S}{\partial V}\right)_T dV + \left(\frac{\partial S}{\partial T}\right)_V dT \tag{47}$$

and

$$dE = \left(\frac{\partial E}{\partial V}\right)_T dV + \left(\frac{\partial E}{\partial T}\right)_V dT \cdot \tag{48}$$

The combined first and second laws of thermodynamics when PdV work is considered is given by

$$TdS = dE + PdV \ .$$

On an isotherm, Eqs. (47) and (48) reduce to the following:

$$dS = \left(\frac{\partial S}{\partial V}\right)_T dV \text{ and } dE = \left(\frac{\partial E}{\partial V}\right)_T dV \ .$$

When these terms are substituted, the TdS equation becomes

$$T\left(\frac{\partial S}{\partial V}\right)_T = \left(\frac{\partial E}{\partial V}\right)_T + P \ . \tag{49}$$

The term $(\partial S/\partial V)_T$ can be written with the aid of Maxwell's equations and the definitions for isothermal bulk modulus B_T and volume expansion coefficient β in the form

$$\left(\frac{\partial S}{\partial V}\right)_T = \left(\frac{\partial S}{\partial P}\right)_T \left(\frac{\partial P}{\partial V}\right)_T = -\left(\frac{\partial V}{\partial T}\right)_P \left(\frac{\partial P}{\partial V}\right)_T = \beta B_T \ .$$

Using this result, Eq. (49) can be expressed in terms of the dependant variable P and the material properties as

$$\left(\frac{\partial E}{\partial V}\right)_T = \beta B_T T - P \ . \tag{50}$$

The pressure and energy in Eq. (46) are regarded as functions of volume on a given isotherm and on the Hugoniot allowing the following to be written,

$$\left(\frac{\partial P}{\partial V}\right)_T = \frac{dP_T}{dV} \ , \ \left(\frac{\partial P}{\partial V}\right)_H = \frac{dP_H}{dV}$$

$$\left(\frac{\partial E}{\partial V}\right)_H = \frac{dE_H}{dV} \ , \ \left(\frac{\partial E}{\partial V}\right)_T = \frac{dE_T}{dV} = \beta B_T T - P_T \ .$$

Substituting the right-hand side of Eq. (38) for the right-hand side of Eq. (46), the differential equation for P_T is expressed as

$$\frac{dP_T}{da} + k(\beta B_T - P_T) = \frac{C^2}{(V_0 - Ma)^3}\left[V_0 + a(M - kV_0)\right] \tag{51}$$

where $a = V_0 - V$. The term $k\beta B_T T$ can be written as

$$k\beta B_T T = k^2 C_V T \tag{52}$$

since

$$k = \Gamma_0 / V_0 = \beta B_T / C_V$$

where C_V is the specific heat at constant volume. This term is constant since k is assumed fixed as defined by Eq. (34), C_V is also taken to be constant, and T is the specified temperature along the isotherm. Eq. (51) can be solved using the integrating factor $\exp(\int k\,da)$ to form

$$P_T = A' e^{ka} + kC_V T + e^{ka} \int \frac{C^2\left[V_0 + a(M - kV_0)\right] e^{-ka}}{(V_0 - Ma)^3}\, da \ . \tag{53}$$

The term containing the integral is identical with that in the expression for the isentrope, Eq. (39). Aided by this information, the solution becomes

$$P_T = A' e^{ka} + kC_V T + P_H + \frac{C^2}{(V_0 - Ma)^2} \sum_{i=3}^{\infty} A_i a^i \tag{54}$$

where A_0, A_1, A_2, and A_i are determined from Eqs. (41) and (42). The constant of integration A' is found from the point at which the isotherm and the Hugoniot curves cross provided T is known. At this point, $P_T = P_H$ and $a = a_H$ so that

$$A' = e^{-ka_H}\left[kC_V T + \frac{C^2}{(V_0 - Ma)^2} \sum_{i=3}^{\infty} A_i a_H^i\right] \ . \tag{55}$$

A fundamental quantity which can be calculated is the temperature on the Hugoniot. From the first TdS equation, assume the functional form S = S(T, V) for entropy so that

$$TdS = T\left(\frac{\partial S}{\partial T}\right)_V dT + T\left(\frac{\partial S}{\partial V}\right)_T dV \ . \tag{56}$$

Since

$$T(\partial S/\partial T)_V = C_V$$

and

$$(\partial S/\partial V)_T = \beta B_T = kC_V$$

then Eq. (56) can be expressed as

$$TdS = C_V dT + kTC_V dV \ . \tag{57}$$

Since dS = 0 on an isentrope, then Eq. (57) reduces to a differential equation for the temperature

$$dT/T = kdV \ . \tag{58}$$

The solution is

$$T = T_i e^{k\alpha} \tag{59}$$

where $\alpha = V_0 - V$ and T_i is some initial temperature on the isentrope. At the point of intersection of the isentrope and the Hugoniot curve, $\alpha = \alpha_H$ and the temperature T refers to the temperature on the Hugoniot. The initial temperature T_i is calculated from the second law of thermodynamics. Fig. 7 illustrates the method. From the second law, the change in energy along an isentrope is given by

$$dE = C_V dT$$

and after integrating, the expression becomes

$$E_i - E_0 = C_V(T_i - T_0) \ .$$

The reference energy state at the foot of the Hugoniot labeled E_0 is defined to be zero and T_0 is room temperature (approximately 300°K).

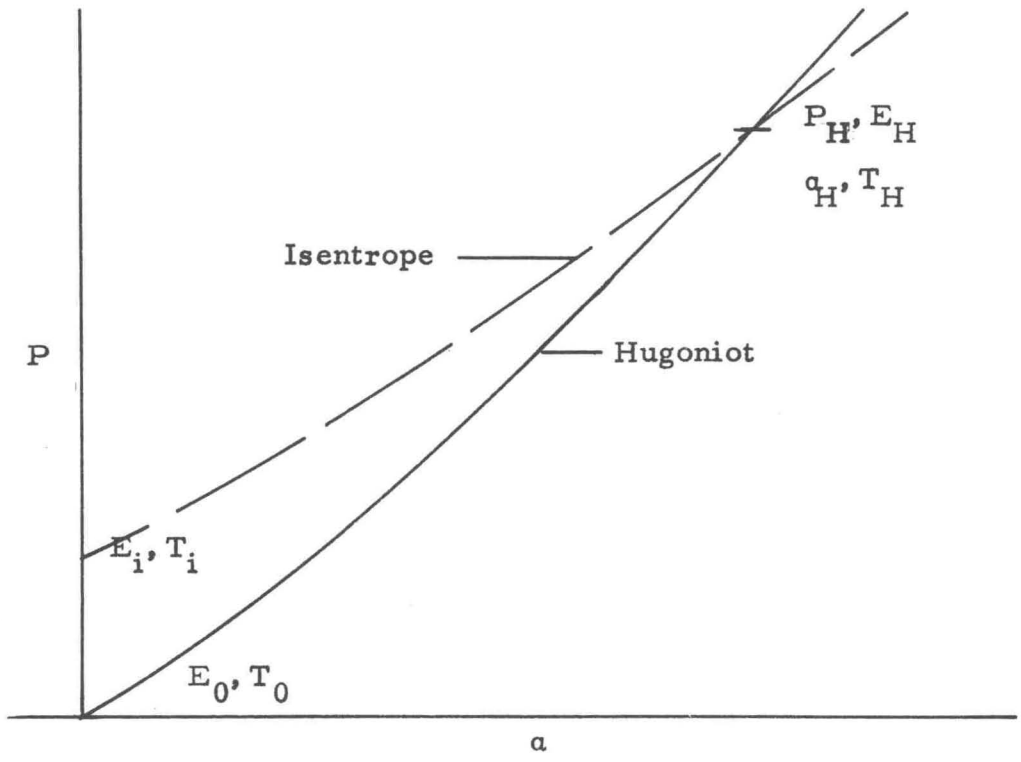

Fig. 7. P-α plot showing a Hugoniot and an isentrope curve.

Hence, the initial temperature can be written as

$$T_i = (E_i/C_V) + T_0 \ . \tag{60}$$

The energy E_S on the isentrope is determined from the differential equation

$$dE_S/d\alpha = P_S \tag{61}$$

where P_S is given by Eq. (43) and the solution to Eq. (61) can be written as a series

$$E_S = \frac{A}{k} e^{k\alpha} + B + \frac{C^2}{(V_0 - M\alpha)} \sum_{i=0}^{\infty} a_i \alpha^i \tag{62}$$

where $a_0 = a_1 = 0$ and

$$a_i = \left[A_{i-1} + (i-2)Ma_{i-1}\right] / iV_0 \quad \text{for } i \geq 2 \ . \tag{63}$$

The constant of integration B is found by letting $E_S = P_H \alpha_H / 2$ on the

Hugoniot, yielding the expression

$$B = \frac{P_H a_H}{2} - \frac{A}{k} e^{k a_H} - \frac{C^2}{(V_0 - M a_H)} \sum_{i=0}^{\infty} a_i a_H^i \qquad (64)$$

where A is given by Eq. (44). The energy E_i can now be determined by setting $a = 0$ and $E_i = E_S$ in Eq. (62) yielding

$$E_i = (A/k) + B. \qquad (65)$$

Substituting this value into Eq. (60) produces a value for T_i required in Eq. (59).

The bulk sound speed C_b of the compressed material behind the shock front can be calculated from the expression

$$C_b = -V\sqrt{(\partial P/\partial V)_S} = (V_0 - a)\sqrt{(\partial P/\partial a)_S} \qquad (66)$$

where the term $(\partial P/\partial a)_S$ is expressed by Eq. (38). Therefore, the sound speed C_H on the Hugoniot becomes upon substitution of $P_S = P_H$ and $a = a_H$

$$C_H^2 = (V_0 - a_H)^2 \left[kP_H + \frac{C^2(V_0 + Ma_H - kV_0 a_H)}{(V_0 - Ma_H)^3} \right] . \qquad (67)$$

In deriving the equations from which isentropes, isotherms, and sound speed are calculated, it is assumed that Γ/V is a constant in the Mie-Gruneisen form for the equation of state. Also, the final expressions obtained for these equations used the experimental fact that U_s and U_p can be described by a linear relation. The determination of the temperature on the Hugoniot has the added assumption that the specific heat C_V is constant for all T which is probably a rather poor assumption. The experimental data for specific heat are usually tabulated as a function of temperature over some temperature range. This C_P data may be converted to C_V by means of Nernst-

Lindemann equation.[31] Another point to be made is that the series solution used here is valid in the range $\rho_0 M\alpha < 1$ as determined from the convergence criterion. This criterion states that the series converges if the ratio of the absolute values of successive terms

$$\frac{\left|A_{i+1}\alpha^{i+1}\right|}{\left|A_i\alpha^i\right|}$$

is smaller than unity for large i. Lastly, it should be mentioned that this development was a joint effort by John Skalyo, Jr. and the author.

III. EXPERIMENTAL TECHNIQUES

A. Explosives

The plane shock waves discussed in Chapter II are generated by detonating chemical explosives. By varying the type of explosive and the experimental arrangement, dynamic pressures of 20-600 kbar in the liquids are achieved. The success of this dynamic technique for producing high pressures is due largely to methods in casting and pressing large homogeneous blocks of explosives and to the development of accurate machining processes.

The solid explosives basic for most experimental uses are TNT (trinitrotoluene), RDX (cyclotrimethylenetrinitramine), and HMX (cyclotetramethylenetetranitramine). In practice, these explosives are mixed with each other in various proportions or mixed with inert binders. Four common explosives, each having a different pressure associated with the detonation front, were used in this program. Baratol, which is a mixture of 76% by weight of barium nitrate a non-reactive material and 24% TNT, has the lowest detonation pressure of the four explosives. The pressure is about 140 kbar and a detonation velocity of 4.9 km/sec. Intermediate pressures are achieved when TNT is used alone. This explosive has a 180 kbar detonation pressure and a velocity of 6.9 km/sec. A mixture of 60% RDX and 40% TNT called Composition B is used for high pressures. The detonation wave in Comp B travels at 8.0 km/sec with a pressure of 290

kbar. The most energetic explosive is PBX-9404 which is a plastic bonded HMX. It has a detonation pressure of 360 kbar and a detonation velocity of 8.8 km/sec.

The slabs of explosives used in an experiment are machined flat and parallel to tolerances of 0.005 cm over a 30 cm diameter. A large portion of the development work on fabrication and machining of explosives has been done by S-Site personnel at the Los Alamos Scientific Laboratory.

A plane detonation front from point initiation is accomplished by an explosive lens fabricated from two different explosives having different detonation velocities. Fig. 8 is a schematic cross section of the explosive lens used in this research, illustrating the relationship of the two components. The geometry chosen allows the faster detonation wave proceeding along the outer cone to keep pace with that of the inner cone. This condition exists when the angle θ has the relationship

$$\theta = \sin^{-1}(D_s/D_f)$$

where D_s is the slow component detonation velocity and D_f is the detonation velocity of the fast component. The lens of Fig. 8 has an angle of 37 1/2 degrees. The wave arriving at the lens face is plane to within 0.1 μsec over 2/3 of the diameter of a 30 cm diameter lens. Combinations of other fast and slow components are possible in a plane wave lens provided the lens angle is properly chosen. The high explosive pad is initiated over its whole surface as the detonation wave arrives at the lens face. This plane detonation wave propagates through the explosive pad and enters the inert materials of the experimental apparatus as a plane shock wave.

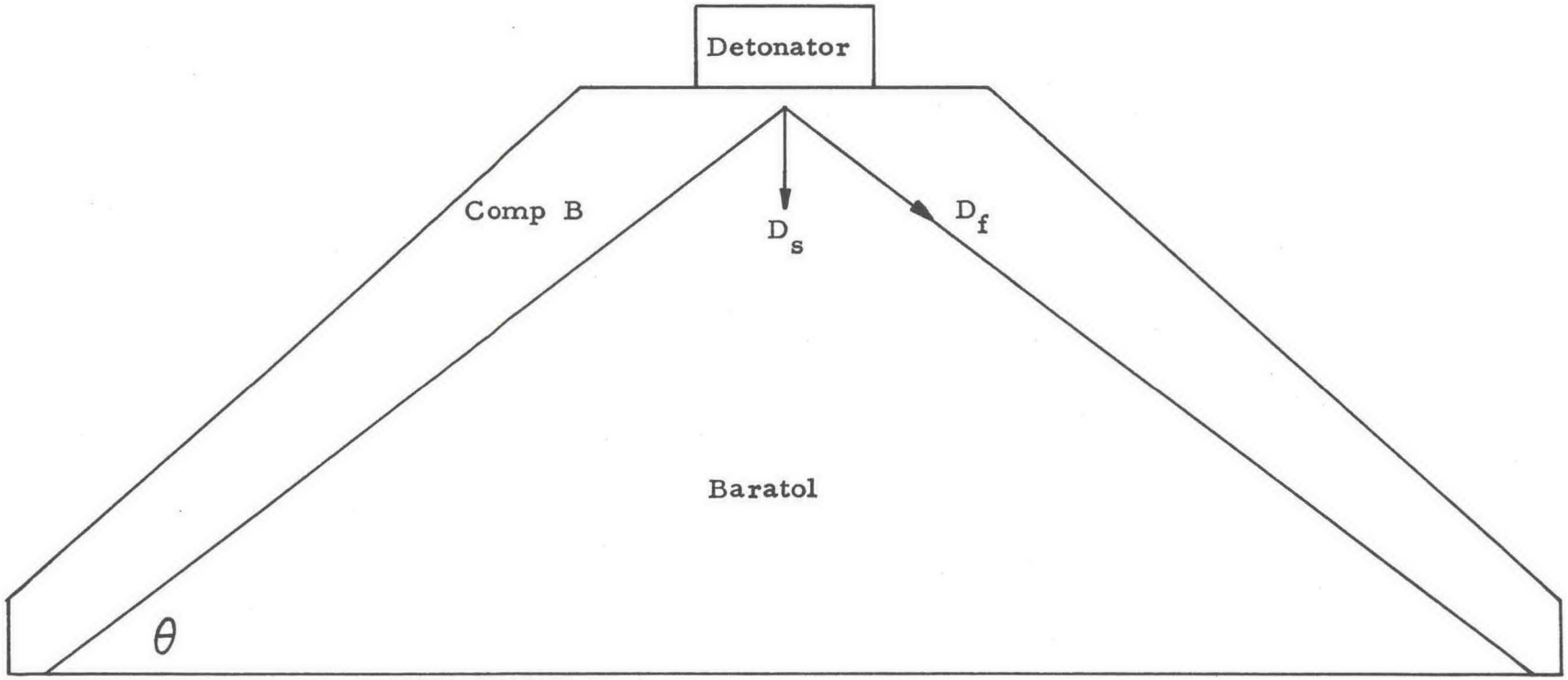

Fig. 8. Typical explosive lens.

B. Electrical Pin Techniques

As mentioned in Chapter II, the Hugoniot can be determined for an unknown sample through a knowledge of the shock and particle velocities and the initial density. The usual procedure for solids is to measure the shock and free surface velocities and then use the free surface approximation, twice the particle velocity equals the free surface velocity, as a first step in an iterative procedure to obtain the particle velocity. Measurement of the shock velocity in the liquids is straightforward but the particle velocity is more difficult to measure. To this end, the impedance-match technique, discussed in Chapter II, affords a convenient means of accurately determining the particle velocity.

The two velocity measuring methods most extensively used in dynamic pressure experiments are electrical pin contactors and high speed camera devices. The optical method was not used in this study and hence will not be discussed. Several accounts are available in the literature.[21-23] The electrical pin contactor,[32,33] commonly called a pin, is an electrical switch that is closed by the action of a shock wave induced motion. With appropriate electronic circuitry and oscilloscope arrangement, the time of closure can be recorded. Electrical pins, as originally used, were designed for solids with good electrical properties but many liquids are normally very good insulators. Consequently, a coaxial pin[34] or self-contained pin was designed to determine the shock velocity in the liquid samples. Fig. 9 is a diagram of the coaxial pin and the associated electronic circuitry. The coaxial pin consists of an insulated center electrode

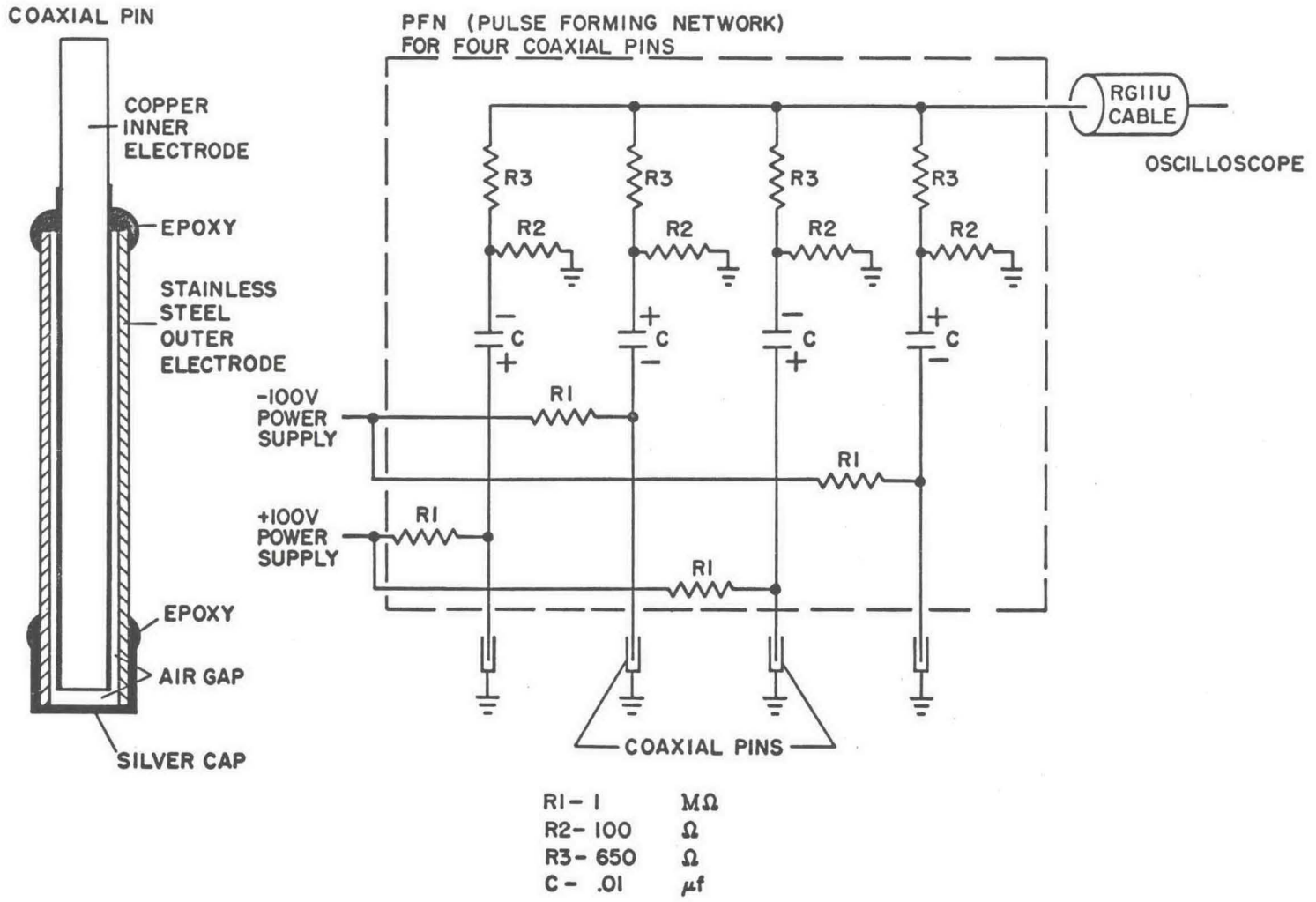

Fig. 9. Diagram of a coaxial pin and the pulse forming network (PFN).

attached to a tubular electrode with a very thin silver foil cap over one end. The inner electrode is set back about 0.0025 cm from the end of the tube and the silver cap. The overall diameter of the completed pin is about 0.09 cm.

When the shock wave strikes the end of the pin, the electrically grounded silver cap is pushed against the charged center wire shorting it to ground. At this instant, the capacitor C discharges and a pulse with a 1 μsec time constant forms across the signal resistor R3. This pulse appears on an oscilloscope trace and is recorded on a glass photographic film plate along with timing and reference pulses. This signal time is closely related to the actual arrival time of the shock front at the pin. By placing pins at selected distances from a reference surface and recording the pin pulses, the shock velocity is determined from the slope of the time-distance data.

C. Shot Construction for the Organic Liquids

Figures 10 and 11 are diagrams of a typical shot assembly used to measure the shock velocities in the ambient temperature liquids and the standard plate. The material chosen for the standard was 2024 dural because the Hugoniot has been previously determined. Dural also has no observed phase transitions below about 1.5 Mbar and is a reasonably good impedance match to the liquids.

The dural plates were machined to 30.5 cm diameter and 1.5 cm thick. In the first quadrant of the plate, flat bottomed holes were drilled to various depths to accept pins for determining the shock velocity. In the second, third, and fourth quadrants, 0.89 cm deep wells were bored for the liquid samples. The bottom of the plate and

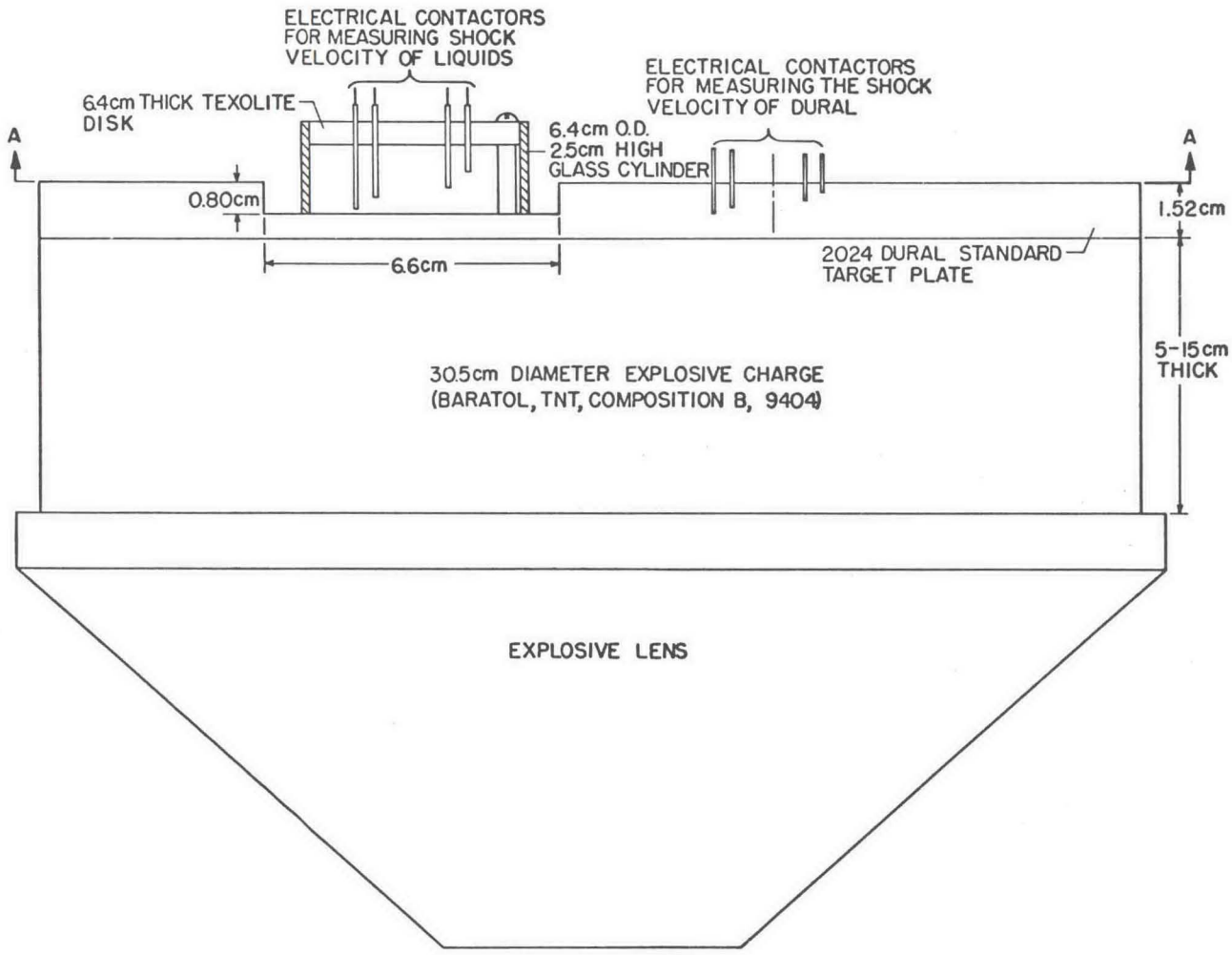

Fig. 10. Section of an experimental assembly for the organic liquids.

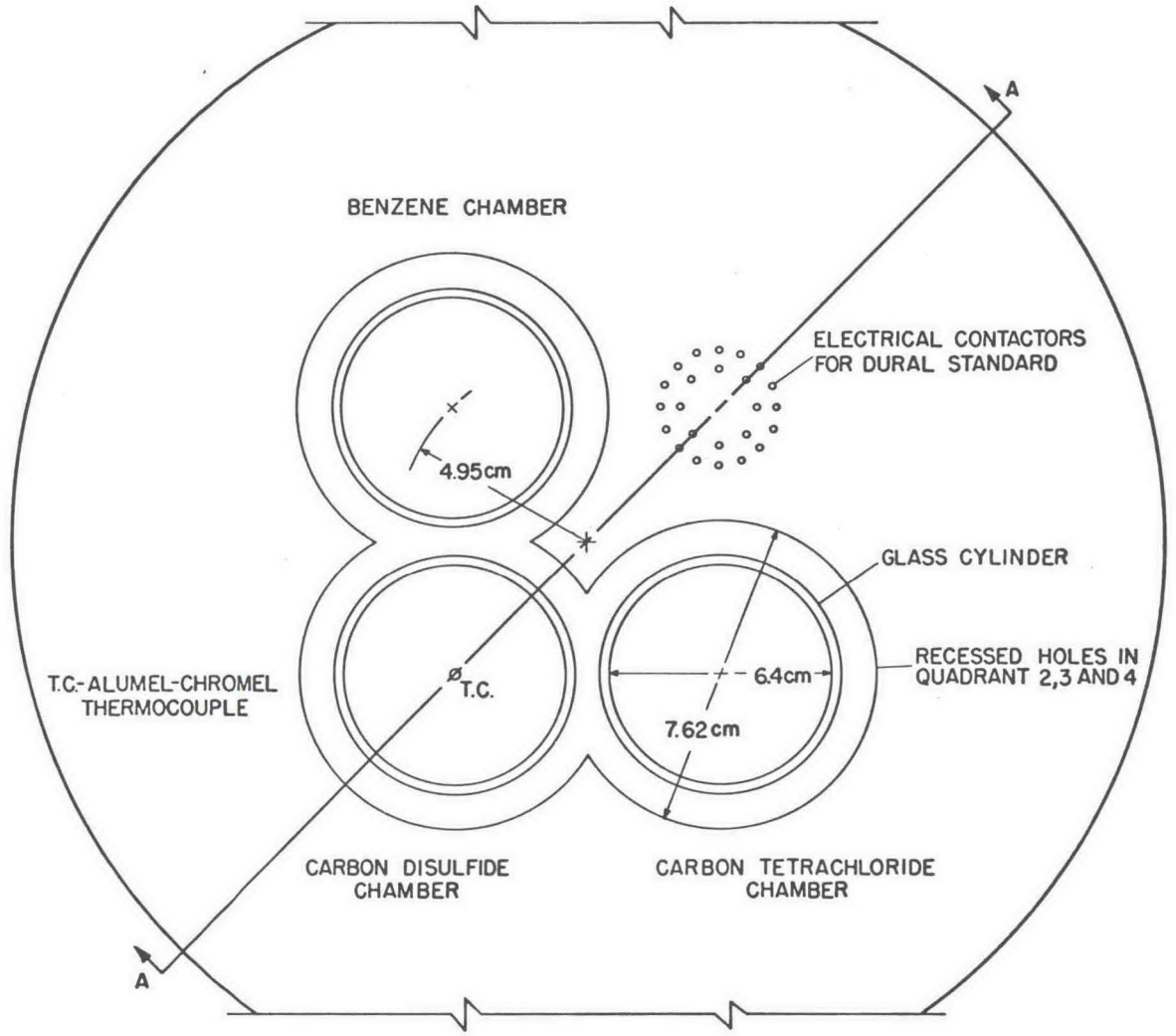

Fig. 11. Top view of Fig. 10.

the bottom of the wells are machined such that the surfaces are flat and parallel to less than 0.0025 cm. Placing the liquids in the three wells allows for measuring the shock front at approximately the same distance from the explosive interface as the shock front in the dural; this tends to keep attenuation differences to a minimum. The pin circles are placed far enough from the edge of the plate and the sides of the wells that the perturbing waves which originate there do not affect the velocity measurements. Using the pin circle arrangement specified in Figs. 10 and 11, the flat bottomed holes are drilled in the dural to specified depths of 0.889, 0.779, 0.559, and 0.459 cm from the top surface with six holes at each of the four depths. The actual depths are obtained by inserting a small diameter steel rod in the hole and measuring the distance it extends above the surface of the surface of the plate. This distance is then subtracted from the known length of the steel rod yielding the actual depth. With this procedure, the hole depths can be measured to a precision of 0.00065 cm. Coaxial pins are then placed in the holes and secured to the plate by epoxy. To prevent movement, each pin is held upright and against the bottom of the hole with a spring loaded jig while the epoxy cures.

In each of the liquids, 24 coaxial pins are arranged on circles of 2.03 and 3.05 cm diameter in a similar manner to the dural. A Textolite disk suspended on three legs 2.5 cm long provides the support for the pins used in each sample. The pins are mounted in holes drilled in the disk and set at distances of 0.01, 0.11, 0.33, and 0.43 cm from the plane defined by the bottom of the three support legs. The actual setbacks are measured to a precision of 0.0007 cm on a comparator after the epoxy around the pins has cured. Then the

glass cylinders shown in Figs. 10 and 11 are epoxied to the bottom of the large recessed wells of the dural plate. The Textolite disks with the pins in them are placed inside the cylinders and screwed to the plate through the support legs.

An electrical lead is then soldered to the center wire of each pin and the braid of the lead is soldered to a bus wire that grounds the outer conductor of the pin. The other ends of the leads are attached to a plug that connects to the PFN circuit. The pins are grouped and identified so that the signals from four pins, one from each level, go to a single oscilloscope. Also, the pins in each group are wired so that the first and third levels have one polarity and the second and fourth levels have the opposite polarity. In this manner, the identity of each signal going to each of the 24 oscilloscopes is known.

An alumel-chromel thermocouple is placed in one of the sample chambers for monitoring the temperature of the liquid at shot time. During the winter months, a heater tape is attached to the dural driver plate to maintain the temperature of the liquids near 20°C.

This completes the laboratory assembly phase of the experiment. In the next phase, the apparatus is taken to a firing point which includes an explosive firing area and a control room in close proximity with interconnecting wiring. It is here that the glass chambers are filled with the proper liquid and the explosive joined to the shot. The thermocouple voltage is monitored on a recorder and if necessary the dural plate is heated. The pin circuits are tested and checked for connection to the correct oscilloscopes. Then the pins are charged to plus or minus 100 volts through the pulse forming

network (PFN). Inside the control room the desired sweep starting times, sweep lengths, and fiducial times are set on all the oscilloscopes. The sweep starts are delayed to allow for explosive burn time and the shock wave time through the inert materials of the experimental apparatus. A typical sweep length is about 6 μsec with the two fiducial pulses placed about 3 μsec apart. The pin pulses will occur between the two fiducials if the shot is correctly timed. Next, glass photographic plates are loaded into the cameras attached to the oscilloscopes and numbered. The calibration trace, which consists of timing markers on the sweep trace, is recorded on the film for each oscilloscope. Then the explosive charge is detonated and as the plane shock wave traverses the assembly, the pins are shorted producing pulses which are recorded on a different portion of the photographic plates. The two fiducial signals also appear with the pin pulses on the trace. In addition, eight raster type oscilloscopes record the firing pulse sent to the detonator as well as the two fiducials; 1/2 μsec timing markers are also recorded on the 100 μsec long raster sweeps. An enlargement of a typical pin signal record and a raster record are presented in Fig. 12.

The next step is to measure the signal times after the film records are developed. Utilizing the known time between timing markers (1/2 μsec) on each record, the time of each pin pulse is measured relative to the fiducials on a precision comparator while the fiducial times are measured from the raster records. These pin times represent the arrival time of the shock wave except for a small closure time assumed to be the same for each pin. This assumption is accurate to 7 nsec. The times are paired with the proper

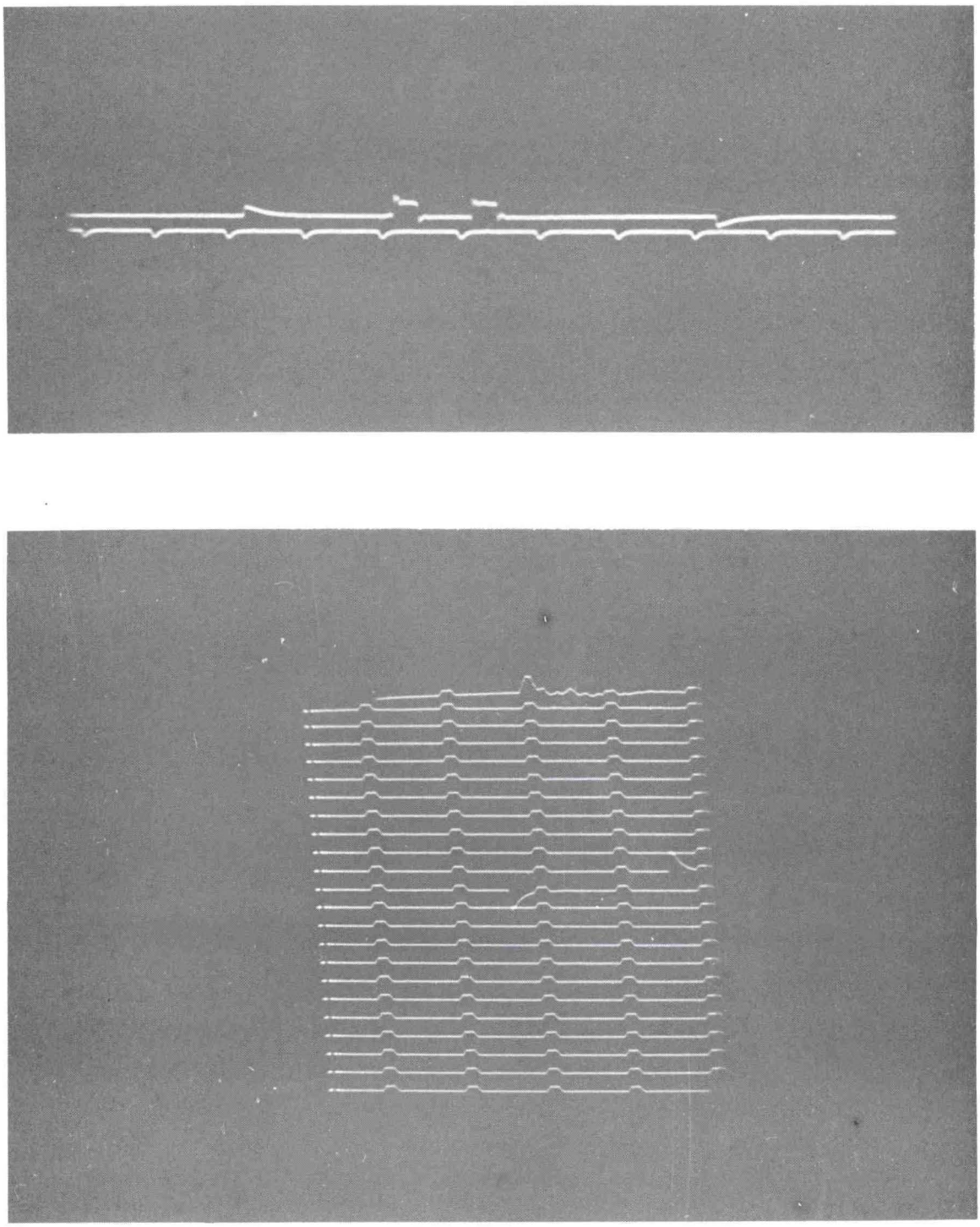

Fig. 12. Typical pin record (top photograph) and raster record (bottom photograph).

pin identity and setback distances. The slope of the time-distance plot then defines the shock velocity. Figure 13 illustrates a typical plot. In practice the velocities are determined by an electronic computer from a linear least squares fit of the time-distance data.

D. Flying Plate Technique

The highest pressures which can be attained in materials in contact with explosives are limited by the highest detonation pressure generated by the explosive and the nature of the material. For instance, PBX-9404 representing the most energetic of the explosives produces a maximum pressure in 2024 dural of about 430 kbar. However, pressures in the megabar range in dural can be achieved by the flying plate or free run technique.[22, 35] This technique consists of accelerating a thin metal plate by a plane wave explosive system and allowing the plate to traverse a two or three centimeter air gap before striking a target plate containing the experimental apparatus.

Consider a metal flyer plate that is very thin compared to the explosive thickness. The shock wave transmitted into the flyer plate from the explosive is reflected from the plate-air interface or free surface as a rarefaction wave. This accelerates the interface to a specific free surface velocity. The release wave travels back through the plate and is reflected at the explosive gas-metal interface as a shock wave and at the same time a rarefaction wave is transmitted into the gas. The reflected shock interacts with free surface again accelerating it to a higher velocity although decreased in incremental magnitude relative to the previous encounter. Successive interactions cause the flyer plate to finally achieve some terminal velocity, U_t,

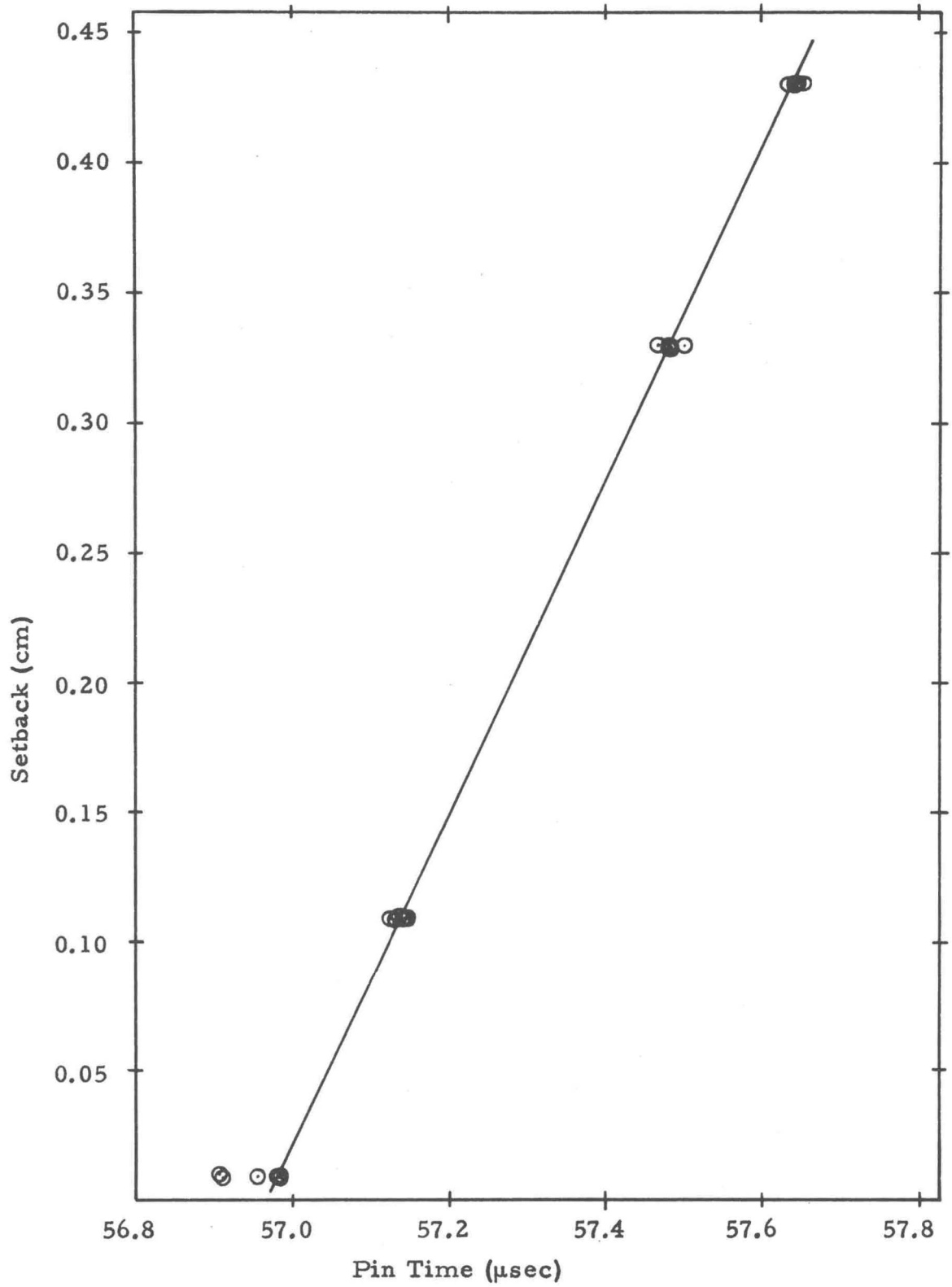

Fig. 13. Typical time-distance plot.

with the plate at zero pressure. Impact causes a shock wave to travel into the target plate and a stopping shock is sent back into the flyer plate as required by the continuity conditions. In the pressure versus particle velocity plane, the state attained in the target plate is defined by the intersection of its Hugoniot curve with the reflected Hugoniot curve for the flyer plate through the point $U_p = U_t$. Assuming identical materials for both the flying plate and the target plate, the particle velocity in the target after impact would be from symmetry one half the terminal velocity of the flying plate. Denser flying plates at the same velocity deliver more momentum to the target giving rise to higher transmitted pressures.

The duration of the pressure pulse in the target depends primarily on the thickness of the flying plate and its sound speed and shock velocity. As an example, the pressure pulse obtained from a 0.16 cm thick stainless steel flying plate is about 1/2 μsec long. A thicker stainless plate increases the time proportionately. This time, called catch-up, represents one round trip through the flying plate plus the time needed for the second transmitted shock wave to overtake the original input wave in the sample. Hence, it is necessary to make the desired velocity measurements before catch-up occurs. If measurements are not accomplished before catch-up, there results a lower measured velocity because the original shock wave is attenuated from the rear by the second wave. A wide range of pressures are possible by choosing various explosives, flying plate densities, thicknesses of the flying plate, and air gap distances. For example, about 1.1 Mbar were achieved in a 0.32 cm thick 2024 dural plate using 15.24 cm thick PBX-9404, a 0.16 cm thick stainless steel plate,

and a 2.54 cm air gap.

The chief difficulties with the flying plate technique are loss in planarity of the shock wave and break-up of the flying plate as it traverses the free run distance. The effects from loss of planarity can be minimized by making the velocity measurements in the materials over as small an area as possible. The break-up can be controlled to some extent by placing a thin layer (approximately 0.03 cm thick) of polyethylene between the explosive pad and the flying plate. A 0.16 cm air gap between the explosive charge and the polyethylene sheet also provides some smoothing of the shock wave sent into the flying plate.

E. Liquid Nitrogen Shot Design

The experimental methods and techniques used in these experiments are similar to the designs used for the organic liquids. To keep the liquid nitrogen in a nonboiling state, a special container was designed. Also, a method was devised so that the container and the explosive charge could be joined remotely from the control room a few seconds before firing the shot. Figure 14 is a schematic diagram of the complete shot assembly. Again the material chosen for a standard target material is 2024 dural.

The dural plate is 25.4 cm in diameter and 10.8 cm thick with a well 0.7 cm deep and 6.35 cm diameter machined in the plate to take the coaxial pins for measuring the liquid nitrogen shock velocity. Small holes are drilled next to this well to take the pins for measuring the dural shock velocity. There are 24 pins for each measurement arranged on two pin circles and four setback levels. The

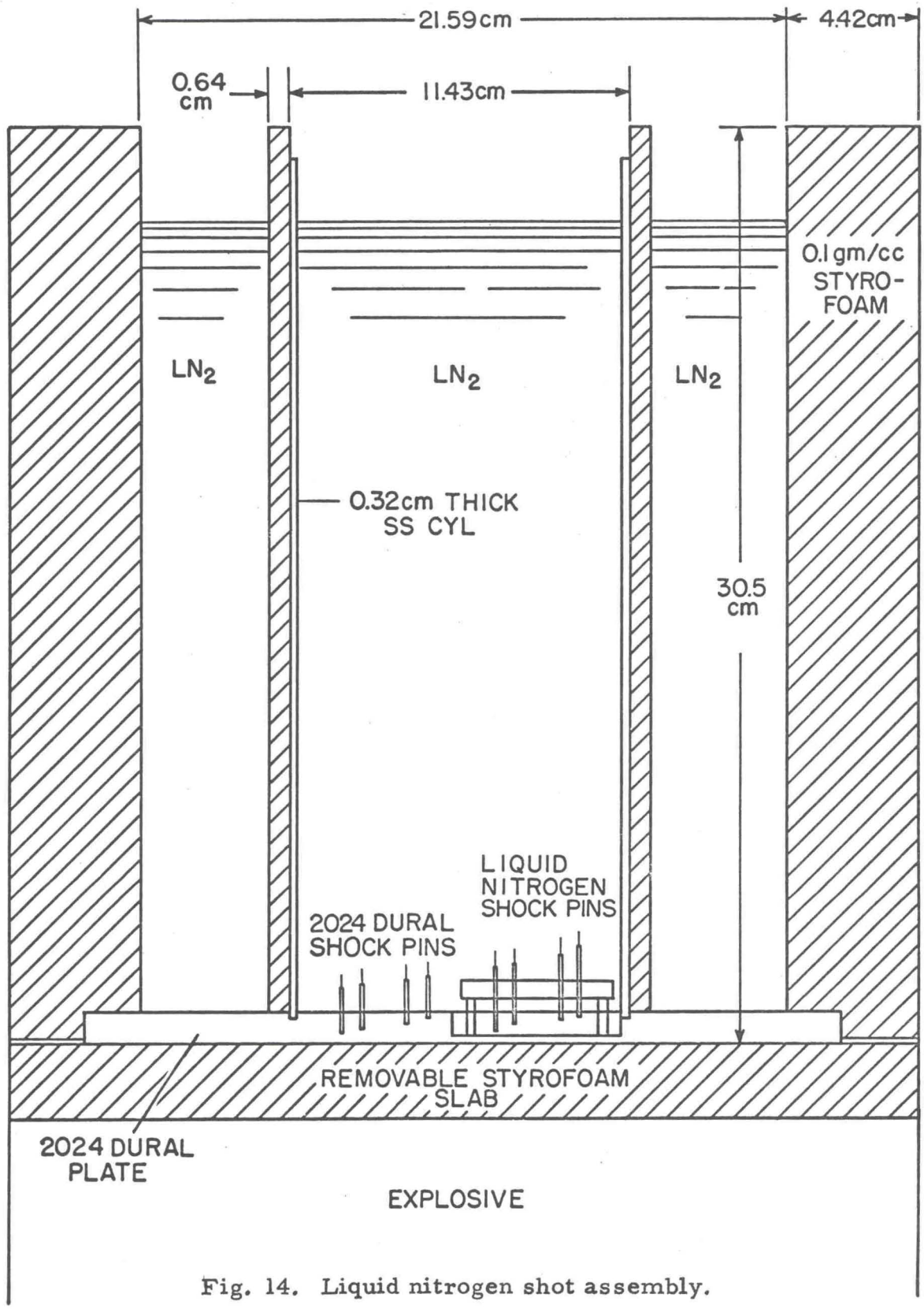

Fig. 14. Liquid nitrogen shot assembly.

hole depths in the dural are 0.76, 0.66, 0.56 and 0.46 cm from the top surface with the deepest hole being the same depth as the well. These hole depths are accurately measured by the method described in Section C. Coaxial pins are inserted in the holes and epoxied in place. The 24 liquid nitrogen shock pins are also arranged in four levels on two pin circles and mounted in a Textolite disk supported on three legs. After setting the pins at specified setbacks of 0.01, 0.11, 0.30 and 0.40 cm from the bottom of the well, they are secured in position and the actual setbacks accurately measured. Then the pin disk is fastened to the well bottom. Electrical leads are soldered to each of the pins with the opposite ends soldered to a plug which connects into the PFN circuit. The pins are grouped such that four pins, one from each level, are connected to an oscilloscope trace. The charging polarity of the pins is alternated in a manner already described.

Then the 11.43 cm diameter stainless steel tube is positioned and epoxied in the groove machined for it. The inner styrofoam cylinder is placed around the steel tube and epoxied to the dural plate. The dural target is positioned into the recess in the large foam cylinder and epoxied. The shot is now ready for final assembly at the firing point.

The container is placed on the removable styrofoam slab and liquid nitrogen poured into the center portion and between the two foam cylinders. After about twenty minutes the liquid nitrogen stops boiling. The assembly, including the foam slab, is then placed on the explosive charge and the usual checks of the shot and electronics are made. To complete the assembly, the foam slab is attached via a steel cable to a lead weight resting on a trap door. When

all is ready in the control room for firing the shot, a solenoid is energized from the control room pulling the solenoid arm free of the trap door allowing it to open. The lead weight falls, jerking the foam slab from between the dural plate and the explosive. This permits the container to drop onto the explosive and at that moment, it closes an electrical switch causing a light to flash on in the control room. The shot is fired at this signal. The interval between the time when the container settles onto the explosive and the time the shot is fired is less than five seconds. This is not sufficient time for the liquid nitrogen to boil.

The electrical pulses generated when the shock wave shorts the pins are recorded on photographic plates along with fiducial pulses and timing markers. The pulse times are measured and paired with the appropriate pins. The shock velocities are then determined from a least squares fit of the time-distance data. A plot of these data is very similar to the illustration of Fig. 13.

A slight modification of the experimental assembly at the firing point is required when flying plate shots are fired. In this case the flying plate with suitable stand-offs is inserted between the explosive and the removable foam slab. A 0.03 cm thick polyethylene sheet is also placed between the explosive and the flying plate. When the foam slab is jerked out, the liquid nitrogen container comes to rest on the stand-offs forming the usual flying plate configuration.

In the shots in which low pressures are desired, brass or uranium attenuator plates 2.54 cm thick are placed between the explosive and the foam disk. The container then comes in contact with the attenuator plate after the foam slab is removed.

IV. EXPERIMENTAL RESULTS AND INTERPRETATION

A. Introduction

There is very little high pressure data available on any chemical compounds initially in the liquid state. This reason, along with interest in development of liquid shot techniques and interest in the liquid state, led to the selection of benzene, carbon disulfide, and carbon tetrachloride. These liquids are readily available in quantity and at relatively high purity. All are non-polar liquids due to configurational symmetry and each has a relatively simple molecular structure.

Liquid nitrogen was included in this investigation primarily for developing experimental apparatus and techniques applicable to other liquids and solids requiring low temperatures to achieve the desired state. To evaluate these developments, the limited Russian Hugoniot work[17] was available for comparison. Liquid nitrogen has the simplest molecular structure of the four liquids, being a diatomic molecule in which the two nitrogen atoms are connected by a triple covalent bond. A purity of about 99.0% was achieved with the major impurity being liquid oxygen. The boiling temperature was determined from vapor pressure tables to be 75°K at local atmospheric pressure. The density at this temperature in the non-boiling state is 0.820 g/cc. The other liquids were obtained from the Mallinckrodt Chemical Works and the General Chemical Division of the Allied Chemical and Dye Corpora-

tion. They were of reagent grade for which purity was at least 99.0%. The benzene molecule is planar and is characterized by the familiar six sided benzene ring with a hydrogen atom attached to each carbon atom through a single covalent bond. The density at 20°C is nominally 0.879 g/cc. Carbon disulfide is a linear tri-atomic molecule in which the C-S bonds are double covalent bonds. At 20°C, the density is 1.263 g/cc. The most dense liquid of the series is carbon tetrachloride at 1.594 g/cc at 20°C. Its molecular configuration is spherical and the single covalent C-Cl bonds are arranged tetrahedrally.

B. Shot Data

The shock Hugoniots for the three organic liquids were determined from thirty-five experiments using the impedance-match technique. As indicated in Figs. 10 and 11, each target plate contained positions for each of the liquids, a position for measuring the dural standard shock velocity, and a thermocouple for determining the initial temperature of the samples at shot time. Table I lists the explosive charge and the metal driver system used for each shot and includes a description of the attenuator and flying plate assemblies. The lens size for all the shots was 30.84 cm diameter except for shot number 12 where a 20.32 cm diameter lens was used. The final driver material in contact with the liquid samples was 2024 dural. The fourth column of Table I lists the dural thickness between the deepest shock pins and the back surface. The dural shock velocities and their standard deviations are tabulated in the last column.

Table I. Shot data for the room temperature liquids.

Shot No.	Explosive[a] and thickness (cm)	Driver system[b] and thickness (cm)	Dural target thickness (cm)	Dural shock vel. (km/sec)
1	10.16 Bor	2.54 Ur	0.51	5.93 ± 0.07
2	10.16 Bar	2.54 Br, 2.54 Lu	0.64	6.02 ± 0.03
3	5.08 Bar	2.54 Ur, 2.54 Du	0.64	6.02 ± 0.04
4	10.16 TNT	2.54 Ur, 2.54 Du	0.64	6.16 ± 0.04
5	10.16 Bar	2.54 Br, 2.54 Du	0.64	6.22 ± 0.03
6	10.16 Bar	1.19 Br, 2.54 Du	0.54	6.23 ± 0.03
7	5.08 TNT	1.27 Br, 1.27 Du	0.64	6.43 ± 0.02
8	10.16 Bar	1.27 Du	0.64	6.50 ± 0.02
9	5.08 Bar	Target plate only	0.54	6.52 ± 0.02
10	10.16 Bar	Target plate only	0.64	6.54 ± 0.02
11	10.16 Bar	1.27 Du	0.51	6.62 ± 0.07
12	5.08 TNT	2.54 Du	0.64	6.78 ± 0.02
13	10.16 TNT	2.54 Du	0.64	6.86 ± 0.01
14	5.08 TNT	Target plate only	0.54	6.92 ± 0.04
15	10.16 TNT	Target plate only	0.64	6.95 ± 0.02
16	5.08 TNT	0.033 Poly, 1.27 Du FP, 2.54 AG	0.32	7.14 ± 0.08
17	10.16 CB	2.54 Du	0.64	7.26 ± 0.01
18	10.16 CB	1.27 Du	0.64	7.31 ± 0.02
19	5.08 CB	Target plate only	0.54	7.35 ± 0.03

Table I. (continued)

Shot No.	Explosive[a] and thickness (cm)	Driver system[b] and thickness (cm)	Dural target thickness (cm)	Dural shock vel. (km/sec)
20	15.24 CB	Target plate only	0.64	7.56 ± 0.03
21	15.24 9404	Target plate only	0.54	7.80 ± 0.03
22	15.24 9404	Target plate only	0.64	7.83 ± 0.02
23	5.08 9404	0.013 Poly, 0.32 Du FP, 1.59 AG, 1.27 Du	0.64	8.20 ± 0.06
24	5.08 9404	0.013 Poly, 0.32 Du FP, 1.59 AG, 1.27 Du	0.64	8.29 ±0.05
25	5.08 9404	0.013 Poly, 0.32 Du FP, 1.59 AG	0.64	8.48 ± 0.03
26	10.16 CB	0.013 Poly, 0.32 SS FP, 2.54 AG	0.32	8.74 ± 0.08
27	15.24 CB	0.013 Poly, 0.32 SS FP, 2.54 AG	0.64	8.97 ± 0.04
28	15.24 CB	0.013 Poly, 0.32 SS FP, 2.54 AG	0.64	9.00 ± 0.06
29	15.24 CB	0.013 Poly, 0.32 SS FP, 2.54 AG	0.32	9.08 ± 0.08
30	10.16 CB	0.013 Poly, 0.16 SS FP, 2.54 AG	0.64	9.39 ± 0.05
31	15.24 CB	0.013 Poly, 0.16 SS FP, 2.54 AG	0.64	9.77 ± 0.06
32	15.24 9404	0.013 Poly, 0.16 SS FP, 2.54 AG	0.64	10.00 ± 0.06
33	15.24 9404	0.013 Poly, 0.16 SS FP, 2.54 AG	0.64	10.17 ± 0.12
34	15.24 9404	0.013 Poly, 0.16 SS FP, 2.54 AG	0.16	10.18 ± 0.10
35	15.24 9404	0.013 Poly, 0.16 SS FP, 2.54 AG	0.32	10.28 ± 0.09

[a]Bor-Boracitol, Bar-Baratol, CB-Composition B, 9404-PBX-9404

[b]Du-Dural, Br-Brass, Lu- Lucite, Ur-Uranium, SS-Stainless Steel, Poly-Ployethylene, AG-Air Gap, FP-Flying Plate

Twenty-one liquid nitrogen shots were performed and the experimental description of each is presented in Table II. The lens size was 30.48 cm diameter on all shots except as noted. The dural thickness under the shock pins is indicated in the fourth column of the table. In four of the shots (numbers 7, 12, 13, and 14), a 0.16 cm air gap was left between the explosive charge and the polyethylene sheet for additional smoothing of the shock wave sent into the flying plate. The measured dural shock velocities recorded in column five have been corrected for thermal contraction of the dural plate and the coaxial pins to 75°K. Also, listed are the standard deviations of the velocity measurements.

Each organic liquid shot was equipped with an alumel-chromel thermocouple for determining the temperature at shot time. This temperature is required in order to determine accurately the initial density of the liquids from volume expansion data. To accomplish this, let V' be the volume at 0°C then the volume V_0 at a temperature T is given by the expansion formula

$$V_0 = V'(1 + AT + BT^2 + CT^3)$$

where Table III gives values of A, B, and C for the temperature range ΔT. The initial densities recorded in Tables IV, V, and VI are corrected for volume expansion using the above formula and the data of Table III.

C. Precision of the Hugoniot Parameters

The pin setbacks and hole depths are measured to an accuracy of 0.0007 cm and the pin pulse times on the film plates are read to 5 nsec. These measuring tolerances provide a fairly

Table II. Shot data for liquid nitrogen.

Shot No.	Explosive[a] and thickness (cm)	Driver system[b] and thickness (cm)	Dural target thickness (cm)	Dural shock vel. (km/sec)
1[c]	10.16 Bar	2.54 Ur	1.14	6.07 ± 0.07
2	5.08 Bar	2.54 Br	1.06	6.24 ± 0.04
3[c]	10.16 Bar	Target plate only	1.14	6.58 ± 0.03
4[c]	10.16 TNT	Target plate only	1.14	6.97 ± 0.03
5[c]	10.16 CB	Target plate only	1.14	7.48 ± 0.02
6[c]	10.16 9404	Target plate only	1.14	7.71 ± 0.02
7	10.16 CB	0.16 AG, 0.033 Poly, 0.66 FP, 2.54 AG	0.32	7.91 ± 0.01
8	5.08 9404	0.033 Poly, 0.32 Du FP, 1.59 AG	0.32	8.48 ± 0.05
9[c]	15.24 9404	0.013 Poly, 0.64 Du FP, 3.18 AG, 0.64 Du	1.14	8.58 ± 0.07
10	15.24 CB	0.013 Poly, 0.32 SS FP, 2.54 AG, 0.32 Du	0.64	8.89 ± 0.06
11	15.24 CB	0.013 Poly, 0.32 SS FP, 2.54 AG, 0.32 Du	0.32	9.13 ± 0.06
12	10.16 CB	0.16 AG, 0.033 Poly, 0.24 SS FP, 2.54 AG	0.32	9.19 ± 0.10
13	15.24 CB	0.16 AG, 0.033 Poly, 0.32 SS FP, 2.54 AG	0.32	9.22 ± 0.06
14	10.16 CB	0.16 AG, 0.033 Poly, 0.20 SS FP, 2.54 AG	0.32	9.35 ± 0.08
15	10.16 CB	0.013 Poly, 0.16 SS FP, 2.54 AG	0.32	9.43 ± 0.07

Table II. (continued)

Shot No.	Explosive[a] and thickness (cm)	Driver system[b] and thickness (cm)	Dural target thickness (cm)	Dural shock vel. (km/sec)
16	7.62 CB	0.013 Poly, 0.16 SS FP, 2.54 AG	0.32	9.44 ± 0.09
17	15.24 CB	0.013 Poly, 0.16 SS FP, 2.54 AG	0.32	9.56 ± 0.06
18[c]	15.24 CB	0.013 Poly, 0.16 SS FP, 2.54 AG, 0.32 Du	0.32	9.71 ± 0.04
19	15.24 CB	0.013 Poly, 0.16 SS FP, 2.54 AG	0.32	9.85 ± 0.09
20	15.24 9404	0.033 Poly, 0.16 SS FP, 2.54 AG	0.32	10.02 ± 0.08
21	15.24 9404	0.013 Poly, 0.16 SS FP, 2.54 AG, 0.32 Du	0.64	10.11 ± 0.10

[a]Bar-Baratol, CB-Composition B, 9404-PBX-9404

[b]Du-2024 Dural, Br-Brass, Ur-Uranium, SS-Stainless Steel, Poly-Polyethylene, AG-Air Gap, FP-Flying Plate

[c]A 20.32 cm diameter lens was used on these shots.

Table III. Volume expansion data[a].

Liquid	$\Delta T(^0C)$	$A(10^{-3})$	$B(10^{-6})$	$C(10^{-8})$	$V(^0C)$
C_6H_6	11 to 81	1.17626	1.27776	0.80648	1.1109
CS_2	-34 to 60	1.13980	1.37065	1.91225	0.7736
CCl_4	0 to 76	1.18384	0.89880	1.35135	0.6126

[a]American Institute of Physics Handbook (McGraw-Hill Book Company, Inc., New York, 1963), 2nd ed., p. 2-159 and 4-75.

precise determination of the shock velocity in the sample and the standard.

Once the time-distance data have been obtained for an experiment, a computer code is used to make a linear least squares fit to this information. The input data required for this program includes the pin pulse time t_i, the pin setbacks or depths z_i, and the pin coordinates x_i and y_i. These data are then fitted by the equation

$$t_i = P_1 + P_2 z_i + P_3 x_i + P_4 y_i$$

where the P coefficients are to be determined. The constants P_3 and P_4 are a measure of the tilt of the shock wave with respect to the plane of the pin circle. The time t_{ci} which represents the time the pins would have discharged had there been no tilt is written as

$$t_{ci} = t_i - P_3 x_i - P_4 y_i = P_1 + P_2 z_i$$

where P_1 represents the intercept on the corrected time axis t_c and P_2 is the slope of the z, t_c points. The reciprocal of this slope is the measured shock velocity. In addition, the computer program calculates the standard deviation associated with the reciprocal of P_2. This is the error quoted in the tables for the measured shock velocities. An additional correction for the dural shock velocities in Table II was made for linear contraction of the dural plate and the coaxial pins when cooled to 75°K. This amounted to about a 0.4% reduction in the originally measured shock velocity. The statistical error varies from 0.1 to 1.2% and generally the larger errors are associated with shots in which thick attenuator plates were used and with flying plate systems in which the flyer plate was relatively thin. It is not the presence of attenuator plates

which causes the larger errors but the low pressures generated by such a system are within the elastic-plastic pressure region of the dural target plate. The elastic wave which precedes the main shock front may be of sufficient strength to short some of the electrical pins prematurely, thereby adding a systematic error to the time-distance points. The errors in the flying plate systems are probably caused by loss of planarity of the shock wave and breakup of the flyer plate.

The transformation of the measured shock velocities and initial density from each sample to pressure-volume data was done by impedance matching to the known dural standard. This was accomplished by a computer program written by John Skalyo, Jr. and Richard H. Warnes of LASL Group GMX-4. The code using the Mie-Gruneisen equation of state along with the conservation relations and continuity conditions provides an analytic solution to the impedance matching problem described graphically in Section E of Chapter II from the experimental data and the dural equation of state information.

The input data required for the program include the initial density and the measured shock velocity for each sample and the 2024 dural standard along with the statistical errors. The equation of state information for the dural standard in the form

$$U_s = C + MU_p$$

and the value for the Gruneisen ratio Γ_0 at $V = V_0$ is also required. The equation of state parameters[26] are $C = 5.460$ km/sec and $M = 1.318$. The dural density is 2.785 g/cc and the value of Γ_0 calculated from Eq. (29) using pure aluminum initial data is 2.22. In the program, Eq. (30) is assumed to hold.

The computer code determines the state to which the dural

was shocked and calculates a release isentrope from that state (see Figs. 5 and 6). Then the velocity given to a dural mass element by the rarefaction wave is calculated and added to the particle velocity associated with the measured shock velocity. The calculation terminates when the release isentrope and the line of slope $\rho_0 U_s$ of the sample intersect. At this point, the particle velocity of the sample is the sum of the particle velocity associated with the shocked state of the dural and the velocity given to the dural mass element by the rarefaction wave. The pressure in the sample is then found from Eq. (8).

The program also calculates the precision index σ_p for the sample particle velocity from the relation

$$\sigma_p = \sqrt{(\sigma_p')^2 + (\sigma_p'')^2}.$$

Here σ_p' is the change in the particle velocity from the calculated value when the sample shock velocity is changed one standard deviation while leaving the dural shock velocity unchanged. σ_p'' represents the difference between a new particle velocity and the mean when the dural shock velocity is changed one standard deviation and the shock velocity of the sample remains unaltered. This same procedure is followed to obtain the precision index for the sample pressure. The expression to calculate the error for the relative volume σ_V of the sample is

$$\sigma_V = \frac{V}{V_0}\sqrt{\left(\frac{\sigma_s}{U_s}\right)^2 + \left(\frac{\sigma_p}{U_p}\right)^2}$$

where U_s, σ_s, U_p, and σ_p are the appropriate velocities and their associated errors. Normally, the statistical error in the particle

velocity (U_p), pressure (P), and relative volume (V/V_0) is about 2% for the organic liquids and slightly larger for liquid nitrogen.

A computer program was written to calculate isentropes, isotherms, and the sound speed and temperature on the Hugoniot. Essentially, the program computes the series solution to the differential equations for the pressure along an isentrope and an isotherm expressed by Eqs. (43) and (54) respectively. It also includes the necessary supporting equations. The code, as written, follows closely the sequence developed in Section F of Chapter II. The temperature on the Hugoniot is calculated from Eq. (59) and the sound speed of the compressed material is determined from Eq. (67). The input data necessary for the program to calculate these thermodynamic quantities are (1) C (intercept from the relation $U_s = C + MU_p$ determined from the experimental data), (2) M (slope of the above linear relationship), (3) Γ_0/V_0 calculated from Eq. (29), (4) thermal expansion coefficient β defined in Eq. (28), (5) $C_P = A + BT + CT^2$, and (6) the initial temperature at the time the experiment was conducted. The initial data required for the computer to perform the calculations are listed in Table IV for all the liquids.

D. Benzene

The Hugoniot data for benzene are listed in Table V. Such data are usually presented graphically on a shock velocity versus particle velocity plot (called a U_s-U_p plot) and pressure versus relative volume (V/V_0) plot (called a P-V/V_0 plot); Figs. 15 and 16 are these plots for benzene.

An examination of the U_s-U_p plot reveals a region of shock velocities from 2.3 to 5.7 km/sec which can be represented by a

Table IV. Input data for thermodynamic calculations by the computer.

Sample	Γ_0/V_0[a]	Density[b] (g/cc)	Coef. of vol. expansion[c] (1/ C)10^{-3}	Specific heat[d, e, f, g] $C_P=A+BT+CT^2$ (ergs/g- K)	Initial temp. (C)	Intercept[h] C (km/sec)	Slope[h] M
C_6H_6	1.06	0.879	1.237	A = 1.52(10^7) B = -1.24(10^4) C = 67.0	293	1.88	1.58
CS_2	1.97	1.263	1.218	A = 1.41(10^7) B = -6.61(10^4) C = 180	293	1.64	1.46
CCl_4	2.00	1.595	1.236	A = 7.81(10^6) B = 2.24(10^3) C = 0	293	1.47	1.57
LN_2	1.77	0.820	6.0	A = 1.74(10^7) B = 4.00(10^4) C = 0	75	1.49	1.49

Table IV. (continued)

[a]Calculated from data in the International Critical Tables (McGraw-Hill Book Company, Inc., New York, 1926) and the American Institute of Physics handbook (McGraw-Hill Book Company, Inc., New York, 1963), 2nd ed.

[b]Calculated from data of Table III for the organic liquids and vapor pressure tables for liquid nitrogen.

[c]Data from the American Institute of Physics Handbook (McGraw-Hill Book Company, Inc., New York, 1963), 2nd ed. for the organic liquids and International Critical Tables (McGraw-Hill Book Company, Inc., 1926) for liquid nitrogen.

[d]Benzene - Rec. Trav. Chim. 74, 1465(1955).

[e]Carbon disulfide - Z. Physik 113, 710(1939).

[f]Carbon tetrachloride - Trans. Faraday Soc. 51, 323(1955).

[g]Liquid nitrogen - JANAF Thermochemical Data Tables Part I.

[h]Listed values are below the transition pressure.

Table V. Shock wave data for the benzene Hugoniot.

Shot No.	Initial temp. (°C)	Initial density (g/cc)	Shock vel. (km/sec)	Particle vel. (km/sec)	Pressure (kbar)	Relative vol. V/V_0
1	22	0.877	2.78 ± 0.01	0.61 ± 0.09	15.0 ± 2.1	0.779 ± 0.031
2	29	0.869	2.72 ± 0.01	0.73 ± 0.04	17.4 ± 1.0	0.730 ± 0.016
3	28	0.870	2.96 ± 0.02	0.73 ± 0.05	18.9 ± 1.2	0.753 ± 0.016
4	28	0.870	3.31 ± 0.01	0.90 ± 0.03	25.8 ± 0.9	0.730 ± 0.009
5	24	0.875	3.44 ± 0.01	0.97 ± 0.03	29.1 ± 1.0	0.719 ± 0.009
6	20	0.879	3.47 ± 0.01	0.98 ± 0.04	29.8 ± 1.2	0.719 ± 0.012
7	19	0.880	3.85 ± 0.01	1.22 ± 0.03	41.3 ± 1.0	0.684 ± 0.008
8	32	0.866	3.89 ± 0.00	1.31 ± 0.02	44.2 ± 0.8	0.663 ± 0.006
9	14	0.885	4.05 ± 0.01	1.31 ± 0.03	47.1 ± 1.0	0.676 ± 0.007
10	22	0.877	4.05 ± 0.01	1.34 ± 0.03	47.6 ± 0.9	0.669 ± 0.006
11	18	0.881	4.09 ± 0.01	1.45 ± 0.09	52.1 ± 3.1	0.646 ± 0.021
12	29	0.869	4.38 ± 0.01	1.63 ± 0.03	62.3 ± 1.0	0.627 ± 0.006
13	29	0.869	4.52 ± 0.01	1.72 ± 0.01	67.4 ± 0.5	0.620 ± 0.003
14	14	0.885	4.79 ± 0.02	1.78 ± 0.05	75.3 ± 2.1	0.630 ± 0.010
15	27	0.871	4.77 ± 0.02	1.81 ± 0.02	75.4 ± 0.9	0.620 ± 0.004
16	28	0.870	5.00 ± 0.02	2.04 ± 0.10	88.7 ± 4.2	0.591 ± 0.020
17	28	0.870	5.28 ± 0.01	2.17 ± 0.02	99.5 ± 0.8	0.589 ± 0.003
18	24	0.875	5.64 ± 0.01	2.21 ± 0.02	106 ± 1	0.596 ± 0.004
19	19	0.880	5.52 ± 0.02	2.26 ± 0.04	110 ± 2	0.591 ± 0.007

Table V. (continued)

Shot No.	Initial temp. (°C)	Initial density (g/cc)	Shock vel. (km/sec)	Particle vel. (km/sec)	Pressure (kbar)	Relative vol. V/V_0
20	30	0.868	5.71 ± 0.01	2.50 ± 0.03	124 ± 2	0.562 ± 0.005
21	12	0.887	6.00 ± 0.03	2.75 ± 0.03	147 ± 2	0.541 ± 0.006
22	27	0.871	5.93 ± 0.02	2.82 ± 0.02	145 ± 1	0.525 ± 0.004
23	23	0.876	6.17 ± 0.02	3.24 ± 0.08	175 ± 4	0.475 ± 0.013
24	28	0.870	6.22 ± 0.04	3.35 ± 0.06	181 ± 3	0.462 ± 0.010
25	28	0.870	6.43 ± 0.03	3.57 ± 0.03	200 ± 2	0.445 ± 0.005
26	25	0.874	6.82 ± 0.06	3.83 ± 0.09	229 ± 6	0.438 ± 0.015
27	19	0.881	7.23 ± 0.01	4.06 ± 0.04	259 ± 3	0.438 ± 0.006
28	26	0.872	7.16 ± 0.03	4.12 ± 0.08	257 ± 5	0.422 ± 0.011
29	27	0.871	7.25 ± 0.03	4.20 ± 0.09	267 ± 6	0.420 ± 0.013
30	24	0.875	7.66 ± 0.05	4.53 ± 0.06	304 ± 4	0.408 ± 0.009
31	23	0.876	8.24 ± 0.05	4.92 ± 0.07	356 ± 5	0.403 ± 0.009
32	23	0.876	8.61 ± 0.04	5.15 ± 0.07	389 ± 6	0.402 ± 0.009
33	18	0.881	8.91 ± 0.07	5.32 ± 0.15	418 ± 12	0.403 ± 0.017
34	27	0.871	8.82 ± 0.08	5.36 ± 0.12	412 ± 10	0.393 ± 0.015
35	25	0.874	8.97 ± 0.06	5.45 ± 0.11	427 ± 9	0.392 ± 0.013

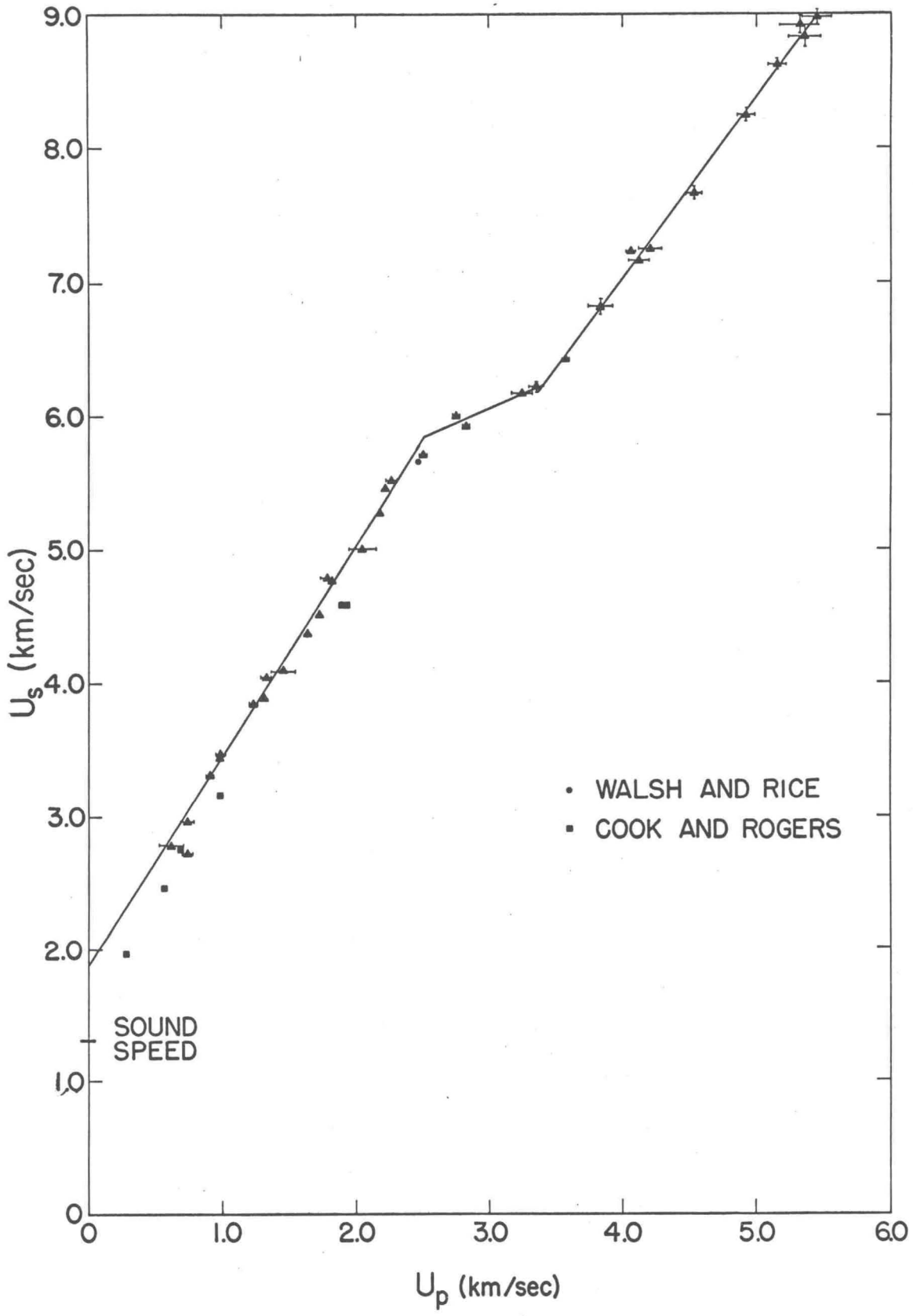

Fig. 15. Benzene shock velocity versus particle velocity.

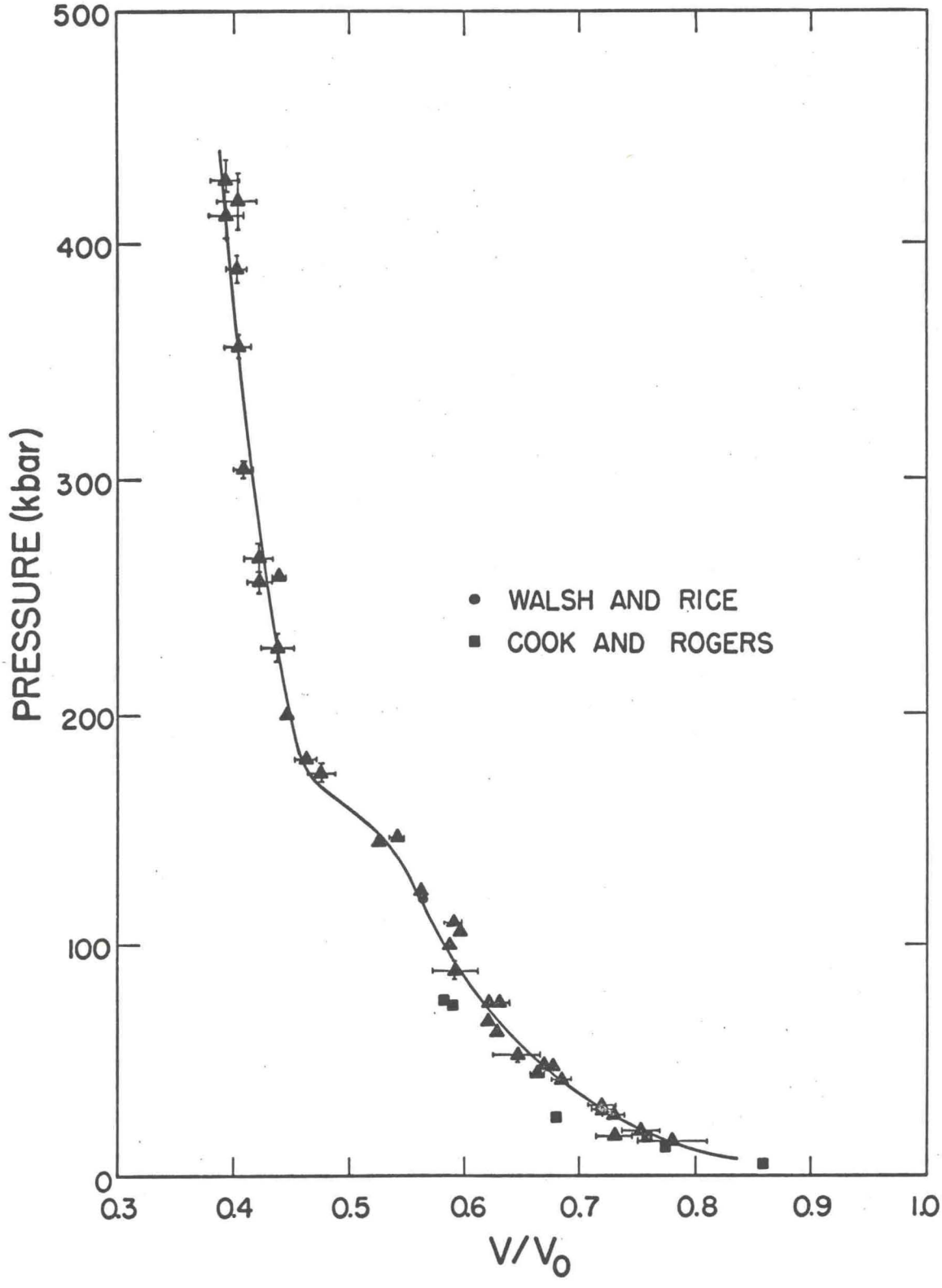

Fig. 16. Benzene pressure versus relative volume.

straight line, a short section from 5.7 to 6.2 km/sec over which the shock velocity increases slowly, and a third region from 6.2 to 9.0 km/sec where the data fits a second straight line. There is very good agreement of the present work with the limited data of Walsh and Rice (reference 14) but the data of Cook and Rogers (reference 16) show a higher particle velocity for a given shock velocity. However, the line through their points parallels the line through the present data. The experimental technique [36] employed by Cook and Rogers was dependent upon direct measurement of the free surface velocity of the liquid by optical methods and invoked the free surface approximation to get the particle velocity. The poor agreement may be due to a condition existing in the liquid similar to spalling in a solid which invalidates the approximation. That is, the compressed liquid separates into very thin layers or a vapor as the shock wave reflects from the free surface and would enhance the free surface velocity.

A linear least squares fit of the U_s-U_p data yields for the lower region

$$U_s = 1.88\pm0.05 + 1.58\pm0.03U_p.$$

From 6.2 to 9.0 km/sec, the data is fit by

$$U_s = 1.68\pm0.12 + 1.34\pm0.03U_p.$$

The middle region was fitted to the following equation,

$$U_s = 4.77\pm0.29 + 0.43\pm0.09U_p.$$

The data of references 14 and 16 were not included in the fit.

From the appearance of the the U_s-U_p plot, it is obvious that the benzene undergoes some type of transition beginning at a shock velocity of 5.7 km/sec. There is also the possibility a second

transition occurs below 2.7 km/sec because the lower line extrapolates to a value on the U_s axis which is higher by 44% than the measured sound velocity*. Bridgman[11] did find that liquid benzene freezes at 0.67 kbar and 25°C and this may account for the poor agreement between the measured sound speed and the extrapolated value.

Fig. 16 is a plot of the data in the pressure-relative volume (P-V/V_0) plane. There is considerable scatter of the points, clouding the actual appearance of the curves. The Hugoniot is drawn as two curves representative of two different phases. The few points between these two phases is shown as fitting a convex upward curve. Both the U_s-U_p plot and the P-V/V_0 plot indicate the transition starts at 125 kbar and ends at 180 kbar. If the upper Hugoniot curve is extrapolated to 125 kbar pressure and the lower curve is used as a reference, the change in V/V_0 due to the transition is about 10%. This large value might be expected from a first order phase change. The two curves were determined from a least squares fit to a third order polynomial with three coefficients. For the upper curve, the equation is

$$P = -103V/V_0 + 155(V/V_0)^2 + 52(V/V_0)^3$$

and for the lower one

$$P = -8V/V_0 + 210(V/V_0)^2 - 6(V/V_0)^3.$$

* Richard Ford of this laboratory measured the sound speeds of benzene, carbon disulfide, and carbon tetrachloride at 22°C and local atmospheric pressure and found them to be 1.31, 1.16, and 0.93 km/sec respectively.

More experimental data are needed in the transition region to accurately map the shape of the Hugoniot curve.

The occurrence of a normal instantaneous transition in a material is reflected in a U_s-U_p plot as a region of constant shock velocity and in this circumstance a two-wave structure is quite likely to be observed.[28, 37] For benzene, the situation is more involved because the U_s-U_p plot reveals a region of slowly increasing shock velocity with particle velocity. A two-wave structure in this situation may still be expected. Duvall[38] treats the case of a P-V Hugoniot described by a concave upward curve connecting at higher pressures to a convex upward curve. This is similar to the benzene case and Duvall predicts this condition will produce a shock wave characteristic of the transition followed by a compression wave. Several experiments were conducted to detect a two-wave structure but the results were inconclusive because of inadequate experimental design. A hydrodynamic calculation in which the experimental arrangement was simulated, indicated that the initial shock wave transmitted into the benzene was overtaken by reflected shock wave from the target plate before the measurement was complete. The calculation was made from a hydrodynamic computer code prepared by Wildon Fickett.

Another explanation of the observed behavior is based on the existence of a metastable Hugoniot and a pressure dependent transition.[37] The original phase is postulated to exist in a metastable condition in the upper phase region and in addition, the larger the overdriving pressure, the farther up the overdriven Hugoniot curve the material goes. Some time later the compressed benzene transforms, allowing the input pressure to relax to the second phase. The

measured shock velocity then reflects this overdrive pressure and as a result there is a region in the U_s-U_p plane where the shock velocity increases slowly. When the material transforms and the pressure relaxes, the shock wave becomes unstable and two shocks form. This explanation seems to generally fit the benzene data. The best answer may be provided by combining the concepts of a metastable Hugoniot and a pressure dependent transition with the idea that a transition region is represented by a convex upward curve in the P-V plane.

The following is an attempt to classify[28, 37] and to provide a plausible explanation for the transition observed in benzene. It is proposed that a first order phase transition has occurred in benzene. It is also proposed that the slope of the pressure-temperature (P-T) phase line is positive as Fig. 17 illustrates. The diagrams apply only to high pressure and temperature phases and do not include any freezing lines. In addition, this picture does not provide any details about the mechanism of the transition.

Freezing to a form of ice of benzene seems unsatisfactory even though the liquid may be in a supercooled condition, because the shock process does not provide enough time for the benzene molecules to arrange themselves in a specific ice structure. Furthermore, compression hinders rotation of the molecules to a specific orientation. The temperature associated with the start of the transition at 125 kbar was calculated to be 2200°K by the computer code described previously. Under these particular conditions of temperature and pressure, the molecular bonds are probably distorted and redistributed to such an extent that a more compact form of benzene is initiated. At 180 kbar, the transformation is complete and the Hugoniot now has the charac-

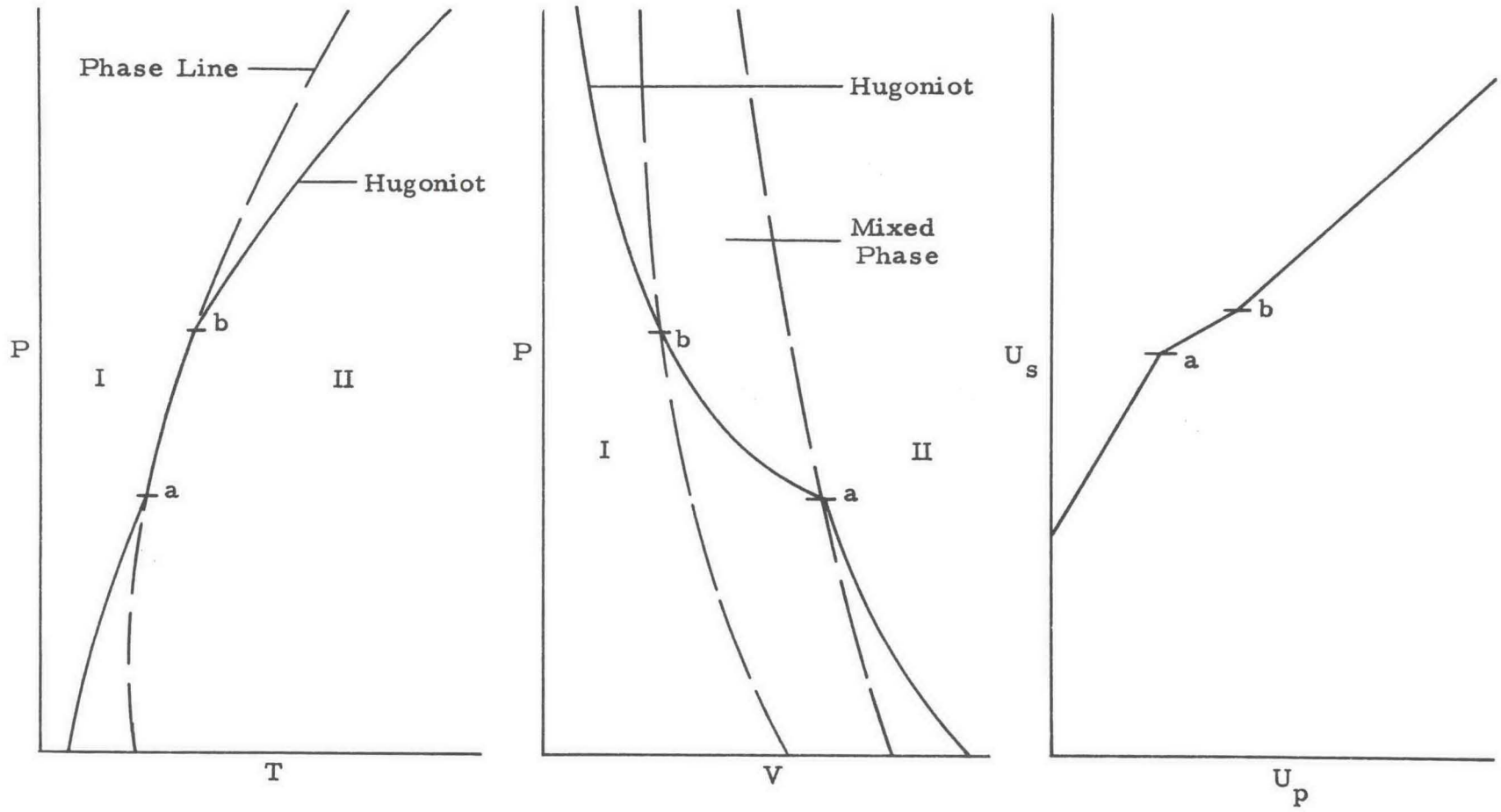

Fig. 17. Ideal phase diagram applied to benzene.

teristics of the high pressure phase. The temperature at this point is probably near 3000°K. Drickamer[39] has concluded from his high pressure work on some solid aromatic hydrocarbons that these compounds undergo crosslinking of the molecular bonds at pressures of 200 kbar and temperatures of 200°K. The Hugoniot of benzene may be influenced by such a mechanism and the elevated temperatures available may actually promote the process.

The results of some crude electrical conduction experiments performed on benzene indicate no appreciable increase in conductivity up to pressures of 140 kbar.

E. Carbon Disulfide

The carbon disulfide data are presented in Table VI and in the shock-particle velocity (U_s-U_p) and the pressure-relative volume (P-V/V_0) planes of Figs. 18 and 19. The data from references 14 and 16 are also plotted.

The carbon disulfide U_s-U_p points fit two straight lines separated by a region of constant shock velocity. On the upper line, the first six points were obtained from experiments in which the explosive was in contact with the driver plate and the remainder from flying plate assemblies. The significance of this observation is that the two lines do accurately describe the behavior of carbon disulfide and are not a result of changing the experimental technique. A comparison of these data with references 14 and 16 indicates the agreement is, in general, poor. The reasons given for the lack of agreement of Cook and Rogers' benzene data probably apply for carbon disulfide also. In addition, many of their points lie in the transition region

Table VI. Shock wave data for the carbon disulfide Hugoniot.

Shot No.	Initial temp. (°C)	Initial density (g/cc)	Shock vel. (km/sec)	Particle vel. (km/sec)	Pressure (kbar)	Relative vol. V/V_0
1	22	1.260	2.47 ± 0.01	0.59 ± 0.08	18.5 ± 2.6	0.761 ± 0.034
2	29	1.249	2.41 ± 0.00	0.71 ± 0.04	21.3 ± 1.3	0.705 ± 0.018
3	28	1.251	2.59 ± 0.01	0.71 ± 0.05	22.9 ± 1.5	0.727 ± 0.018
4	28	1.251	2.94 ± 0.01	0.86 ± 0.03	31.6 ± 1.1	0.707 ± 0.010
5	24	1.257	3.06 ± 0.01	0.93 ± 0.03	35.7 ± 1.2	0.696 ± 0.010
6	20	1.263	3.09 ± 0.01	0.94 ± 0.04	36.5 ± 1.5	0.697 ± 0.012
7	19	1.264	3.39 ± 0.01	1.17 ± 0.03	50.0 ± 1.2	0.655 ± 0.008
8	32	1.245	3.43 ± 0.01	1.26 ± 0.02	53.6 ± 0.9	0.634 ± 0.006
9	14	1.272	3.47 ± 0.01	1.26 ± 0.01	55.8 ± 1.1	0.636 ± 0.008
10	22	1.260	3.47 ± 0.01	1.29 ± 0.02	56.4 ± 1.1	0.628 ± 0.007
11	18	1.266	3.51 ± 0.01	1.39 ± 0.08	61.9 ± 3.8	0.603 ± 0.024
12	29	1.249	3.52 ± 0.01	1.59 ± 0.03	70.1 ± 1.1	0.549 ± 0.007
13	29	1.249	3.55 ± 0.01	1.68 ± 0.01	74.4 ± 0.6	0.527 ± 0.004
14	14	1.272	3.65 ± 0.01	1.74 ± 0.05	81.0 ± 2.2	0.523 ± 0.013
15	27	1.253	3.62 ± 0.01	1.78 ± 0.02	80.9 ± 0.9	0.507 ± 0.006
16	28	1.251	3.78 ± 0.01	2.01 ± 0.10	94.8 ± 4.5	0.468 ± 0.025
17	28	1.251	4.02 ± 0.01	2.13 ± 0.02	107 ± 1	0.471 ± 0.004
18	24	1.257	4.18 ± 0.00	2.17 ± 0.02	114 ± 1	0.481 ± 0.004
19	19	1.264	4.20 ± 0.01	2.22 ± 0.04	118 ± 2	0.473 ± 0.009

Table VI. (continued)

Shot No.	Initial temp. (°C)	Initial density (g/cc)	Shock vel. (km/sec)	Particle vel. (km/sec)	Pressure (kbar)	Relative vol. V/V_0
20	30	1.248	4.40 ± 0.01	2.45 ± 0.03	134 ± 2	0.444 ± 0.003
21	12	1.275	4.86 ± 0.02	2.67 ± 0.03	165 ± 2	0.451 ± 0.007
22	27	1.253	4.80 ± 0.01	2.73 ± 0.02	164 ± 1	0.432 ± 0.005
23	23	1.258	5.23 ± 0.02	3.11 ± 0.08	204 ± 5	0.406 ± 0.015
24	28	1.251	5.20 ± 0.02	3.22 ± 0.06	209 ± 4	0.382 ± 0.011
25	28	1.251	5.68 ± 0.03	3.39 ± 0.03	241 ± 2	0.403 ± 0.006
26	25	1.255	6.04 ± 0.03	3.64 ± 0.09	276 ± 7	0.398 ± 0.015
27	19	1.266	6.46 ± 0.02	3.84 ± 0.04	314 ± 4	0.406 ± 0.007
28	26	1.254	6.36 ± 0.02	3.90 ± 0.07	311 ± 6	0.388 ± 0.011
29	27	1.253	6.44 ± 0.04	3.98 ± 0.09	321 ± 7	0.383 ± 0.015
30	24	1.257	6.73 ± 0.03	4.30 ± 0.09	364 ± 5	0.361 ± 0.010
31	23	1.258	7.34 ± 0.04	4.65 ± 0.07	429 ± 6	0.366 ± 0.010
32	23	1.258	7.64 ± 0.05	4.87 ± 0.07	468 ± 7	0.362 ± 0.010
33	18	1.266	7.83 ± 0.03	5.03 ± 0.14	499 ± 14	0.357 ± 0.018
34	27	1.253	7.98 ± 0.08	5.03 ± 0.12	503 ± 12	0.370 ± 0.017
35	25	1.255	8.09 ± 0.05	5.12 ± 0.11	520 ± 11	0.367 ± 0.014

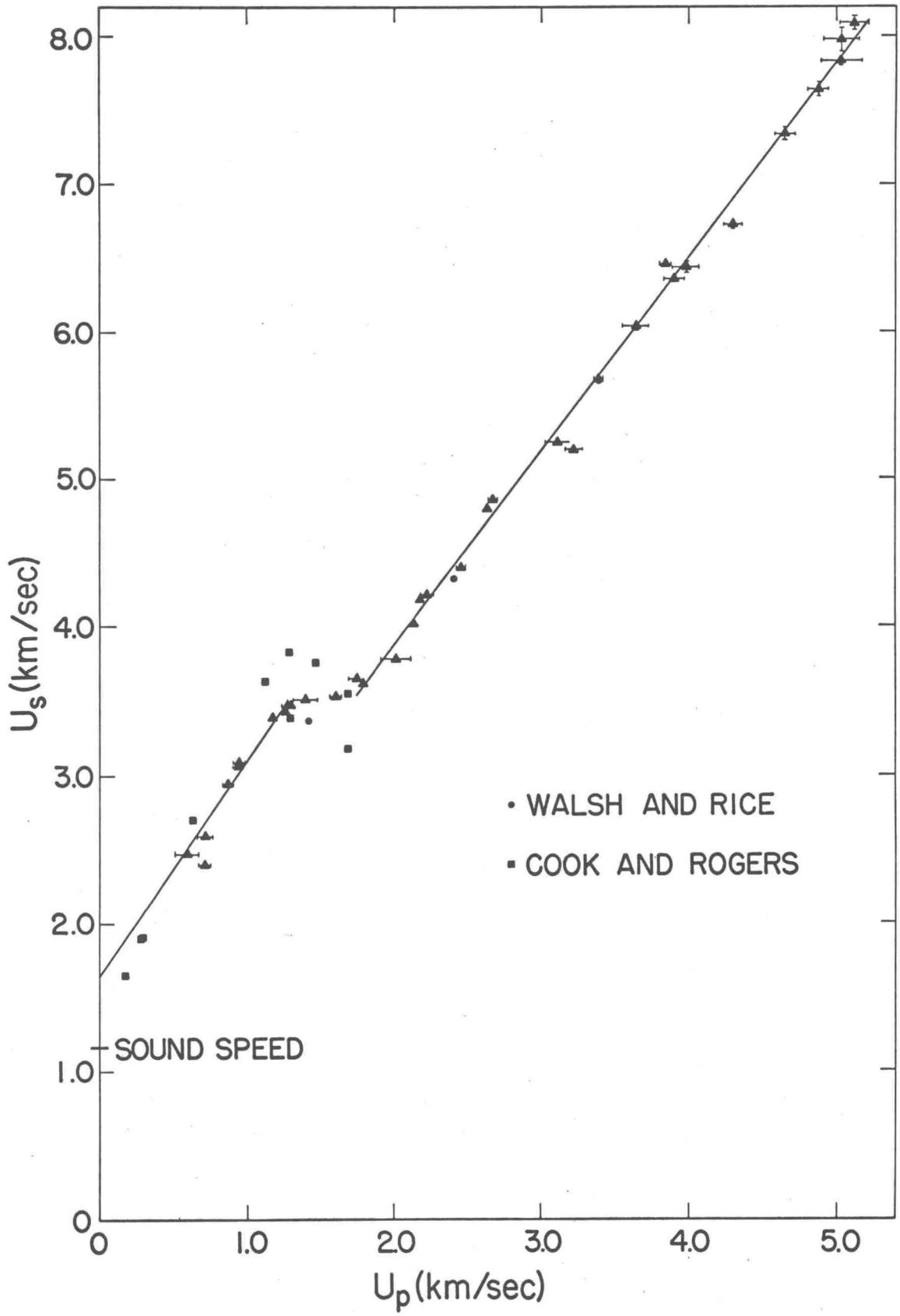

Fig. 18. Carbon disulfide shock velocity versus particle velocity.

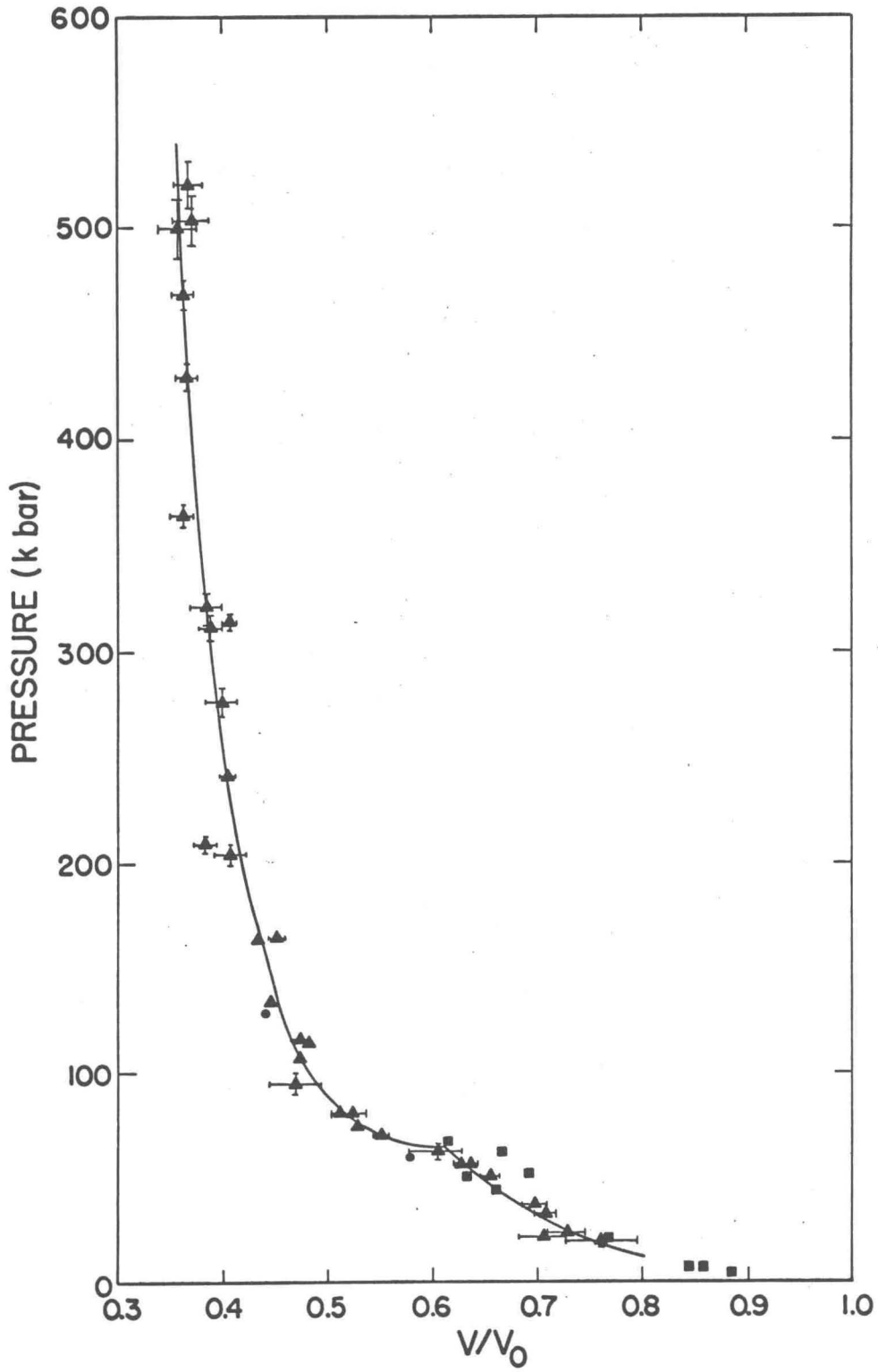

Fig. 19. Carbon disulfide pressure versus relative volume.

which may account for additional error.

The lower U_s-U_p data were found to fit the expression

$$U_s = 1.64 \pm 0.08 + 1.46 \pm 0.08 U_p$$

in the shock velocity range of 2.4 to 3.5 km/sec and the upper line from 3.5 to 8.1 km/sec fits the line

$$U_s = 1.25 \pm 0.06 + 1.32 \pm 0.02 U_p.$$

In the particle velocity interval 1.3 to 1.8 km/sec, the shock velocity is essentially constant. An extrapolation of the lower line to zero particle velocity yields a velocity which is about 40% higher than the measured sound speed suggesting a transition below 20 kbar. The obvious break at a shock velocity of 3.5 km/sec is the type of behavior observed when a solid undergoes a phase transition.

A plot of the P-V/V_0 data presented in Fig. 19 indicates two concave upward curves with a cusp at 64 kbar. The scatter is quite noticeable and causes some difficulty in describing the data with accurate curves. The location of the transition cusp is fairly well defined, especially when using the U_s-U_p information. Based on a knowledge of shape of the isotherm for static pressures in the neighborhood of a transition, a rough estimate of the decrease in volume is 15%. The data in the 20-65 kbar pressure range were fit by the least squares method resulting in the expression

$$P = 10V/V_0 + 139(V/V_0)^2 + 3(V/V_0)^3.$$

From 130 to 520 kbar, the data fit the expression

$$P = 60V/V_0 - 879(V/V_0)^2 + 394(V/V_0)^3.$$

A French curve was used to draw the curve through the remaining data between 65 and 130 kbar.

Carbon disulfide probably undergoes a normal first order

phase transition at 64 kbar. The evidence supporting this hypothesis is (1) a region in the U_s-U_p plane over which the shock velocity is constant, (2) the Rayleigh line connecting the zero pressure point and which goes through the transition cusp intersects the upper P-V curve at a point corresponding to the start of the upper line of the U_s-U_p plot, and (3) the P-V/V_0 Hugoniot curve exhibits a cusp at 64 kbar in agreement with the U_s-U_p data. It is very likely that a two-wave structure accompanies this transition. Experiments to test this suggestion were inconclusive for reasons discussed in the benzene section.

Two very crude experiments were performed to obtain some qualitative information about the electrical conduction of carbon disulfide near the transition region. In one experiment using a 10.16 cm thick Baratol charge, it was observed from rather insensitive instrumentation that there was negligible electrical conduction when underdriving the transition. In the other experiment, a 5.08 cm thick TNT charge was used to shock the carbon disulfide to a pressure slightly above the transition and in this case appreciable electrical conduction was observed. Carbon disulfide at standard pressure and temperature normally is a good insulator but the conductivity increases rapidly upon the application of dynamic pressures. The transformation process may enhance the change in conductivity.

The observed transition is thought to be the transformation of the liquid to a "black substance". This was first discovered by Bridgman[10] and later investigated more fully by Whalley[40] and Butcher and coworkers[41] using static pressure methods. The transformation was found to occur at about 40 kbar over a temperature

range of 120 to 200°C. The substance is black, stable under normal conditions, an amorphous like structure, probably a semiconductor, and has other physical properties reported in the above references. Some explosive recovery experiments[42] conducted at LRL at Livermore have revealed the presence of a black fluffy material after shocking liquid carbon disulfide to about 200 kbar pressure. If the recovered material is indeed carbon disulfide this would support the hypothesis that the liquid phase is being transformed to the so-called black substance under dynamic conditions. The temperature on the Hugoniot at 64 kbar was calculated to be about 1000°K. This provides an additional point for the phase diagram for carbon disulfide.

F. Carbon Tetrachloride

Carbon tetrachloride, in some respects, has a less complicated behavior under shock conditions than either benzene or carbon disulfide. A shock versus particle velocity (U_s-U_p) plot of the data listed in Table VII is shown in Fig. 20 to fit two straight lines. This differs from similar plots of the other two liquids in that the upper line is not displaced relative to the lower line. A linear least square fit of the data in the shock velocity range 2.3 to 4.7 km/sec yields

$$U_s = 1.47\pm0.05 + 1.57\pm0.03U_p$$

and above 4.7 km/sec the linear relationship is

$$U_s = 1.97\pm0.13 + 1.31\pm0.03U_p.$$

The points are not sufficiently precise to preclude the possibility of a smooth curve fitting the data equally well. A least squares fit of the data to a quadratic in U_p results in the equation

Table VII . Shock wave data for the carbon tetrachloride Hugoniot.

Shot No.	Initial temp. (°C)	Initial density (g/cc)	Shock vel. (km/sec)	Particle vel. (km/sec)	Pressure (kbar)	Relative vol. V/V_0
1	22	1.590	2.32 ± 0.01	0.58 ± 0.08	21.3 ± 3.0	0.752 ± 0.035
2	29	1.577	2.27 ± 0.01	0.69 ± 0.04	24.7 ± 1.5	0.697 ± 0.018
3	28	1.571	2.47 ± 0.01	0.69 ± 0.04	26.6 ± 1.7	0.722 ± 0.018
4	28	1.571	2.79 ± 0.01	0.82 ± 0.02	36.4 ± 1.2	0.702 ± 0.010
5	24	1.586	2.91 ± 0.01	0.90 ± 0.03	41.3 ± 1.4	0.692 ± 0.010
6	20	1.594	2.95 ± 0.01	0.90 ± 0.04	42.3 ± 1.7	0.694 ± 0.013
7	19	1.596	3.28 ± 0.01	1.12 ± 0.03	58.7 ± 1.4	0.658 ± 0.008
8	32	1.571	3.32 ± 0.01	1.20 ± 0.02	62.8 ± 1.1	0.637 ± 0.006
9	14	1.606	3.46 ± 0.01	1.20 ± 0.03	66.7 ± 1.4	0.652 ± 0.007
10	22	1.591	3.44 ± 0.01	1.23 ± 0.02	67.4 ± 1.3	0.643 ± 0.007
11	18	1.598	3.50 ± 0.01	1.33 ± 0.08	74.0 ± 4.5	0.621 ± 0.023
12	29	1.577	3.74 ± 0.01	1.49 ± 0.02	88.1 ± 1.4	0.601 ± 0.006
13	29	1.571	3.86 ± 0.01	1.57 ± 0.01	95.1 ± 0.7	0.594 ± 0.003
14	14	1.606	4.08 ± 0.01	1.61 ± 0.05	106 ± 3	0.604 ± 0.011
15	27	1.580	4.07 ± 0.01	1.65 ± 0.02	106 ± 1	0.596 ± 0.005
16	28	1.571	4.27 ± 0.03	1.86 ± 0.09	125 ± 6	0.565 ± 0.021
17	28	1.571	4.52 ± 0.01	1.96 ± 0.02	140 ± 1	0.566 ± 0.003
18	24	1.586	4.66 ± 0.01	2.00 ± 0.02	148 ± 1	0.572 ± 0.004
19	19	1.596	4.71 ± 0.01	2.04 ± 0.04	153 ± 3	0.566 ± 0.008

Table VII. (continued)

Shot No.	Initial temp. (°C)	Initial density (g/cc)	Shock vel. (km/sec)	Particle vel. (km/sec)	Pressure (kbar)	Relative vol. V/V_0
20	30	1.574	4.88 ± 0.01	2.26 ± 0.03	174 ± 2	0.537 ± 0.006
21	12	1.610	5.34 ± 0.02	2.46 ± 0.03	211 ± 2	0.540 ± 0.005
22	27	1.580	5.21 ± 0.01	2.53 ± 0.02	208 ± 2	0.515 ± 0.004
23	23	1.588	5.72 ± 0.03	2.87 ± 0.07	260 ± 7	0.499 ± 0.003
24	28	1.571	5.69 ± 0.02	2.98 ± 0.05	266 ± 5	0.477 ± 0.009
25	28	1.571	6.13 ± 0.03	3.13 ± 0.03	303 ± 3	0.489 ± 0.005
26	25	1.584	6.44 ± 0.05	3.37 ± 0.09	344 ± 9	0.478 ± 0.014
27	19	1.598	6.80 ± 0.02	3.56 ± 0.04	387 ± 4	0.476 ± 0.006
28	26	1.582	6.72 ± 0.02	3.62 ± 0.02	384 ± 7	0.461 ± 0.010
29	27	1.580	6.78 ± 0.03	3.70 ± 0.09	396 ± 9	0.455 ± 0.013
30	24	1.586	7.13 ± 0.03	3.98 ± 0.06	450 ± 7	0.441 ± 0.009
31	23	1.588	7.55 ± 0.02	4.34 ± 0.06	520 ± 8	0.425 ± 0.009
32	23	1.588	7.96 ± 0.03	4.52 ± 0.06	572 ± 8	0.432 ± 0.009
33	18	1.598	8.06 ± 0.06	4.69 ± 0.13	604 ± 17	0.418 ± 0.017
34	27	1.580	8.24 ± 0.04	4.69 ± 0.11	610 ± 14	0.431 ± 0.014
35	25	1.584	8.26 ± 0.03	4.79 ± 0.10	626 ± 13	0.421 ± 0.013

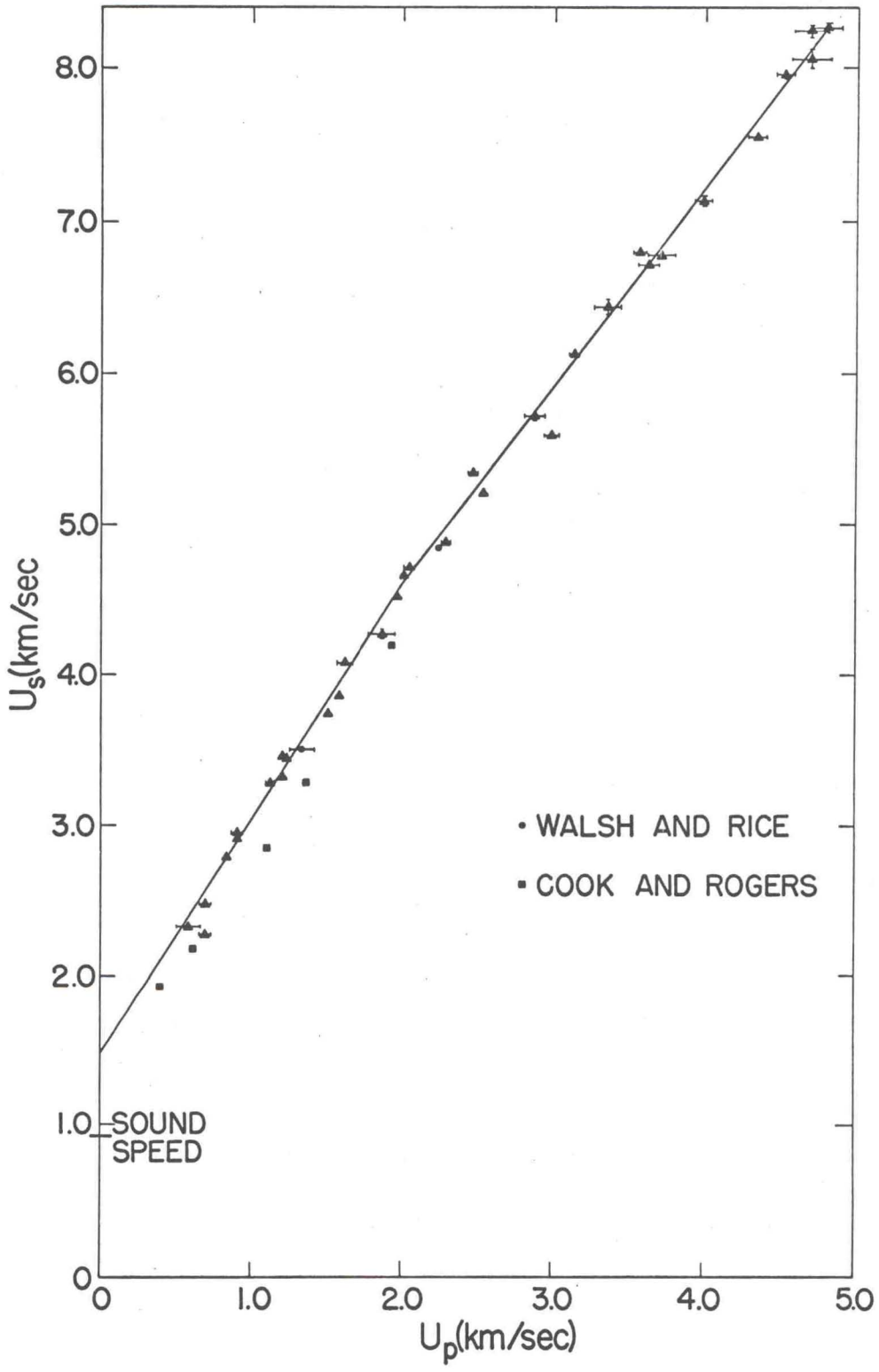

Fig. 20. Carbon tetrachloride shock velocity versus particle velocity.

$$U_s = 1.45\pm0.06 + 1.65\pm0.05U_p - 0.04\pm0.01U_p^2.$$

There is good agreement between the present data and that of Walsh and Rice.[14] Again the data of Cook and Rogers[16] are located toward higher particle velocities, probably for the same reasons discussed previously. However, their points do fit a line which closely parallels the fitted lower line. Like the other two liquids, the extrapolated U_s-U_p line to zero particle velocity intersects the U_s axis at a velocity which is about 60% higher than the measured sound speed. Bridgman[11] found that liquid carbon tetrachloride freezes at about 1 kbar and 25°C which may account for the discrepancy.

Figure 21 is a pressure versus relative volume (P-V/V_0) plot of the data. A simple concave upward curve seems to adequately describe all the points. The lack of precision and scatter of the data prevents establishing a change in slope of the P-V/V_0 curve associated with the break in the linear relationship specified for the U_s-U_p plane. The least squares fitted equation that describes the curve is

$$P = 0.2V/V_0 + 128(V/V_0)^2 + 133(V/V_0)^3.$$

Since the carbon tetrachloride U_s-U_p plot did not exhibit a region of constant shock velocity and the P-V/V_0 curve did not show a transition cusp, it was assumed that a two-wave structure was nonexistent and no two-wave experiments were performed.

In some early experiments[43] on shock induced electrical conduction of carbon tetrachloride, it was found that between 100 and 150 kbar the conductivity was increased sufficiently to short out a charged bare wire pin at the arrival time of the shock wave. Walsh and Rice[14] even earlier reported a change in transparency to visible

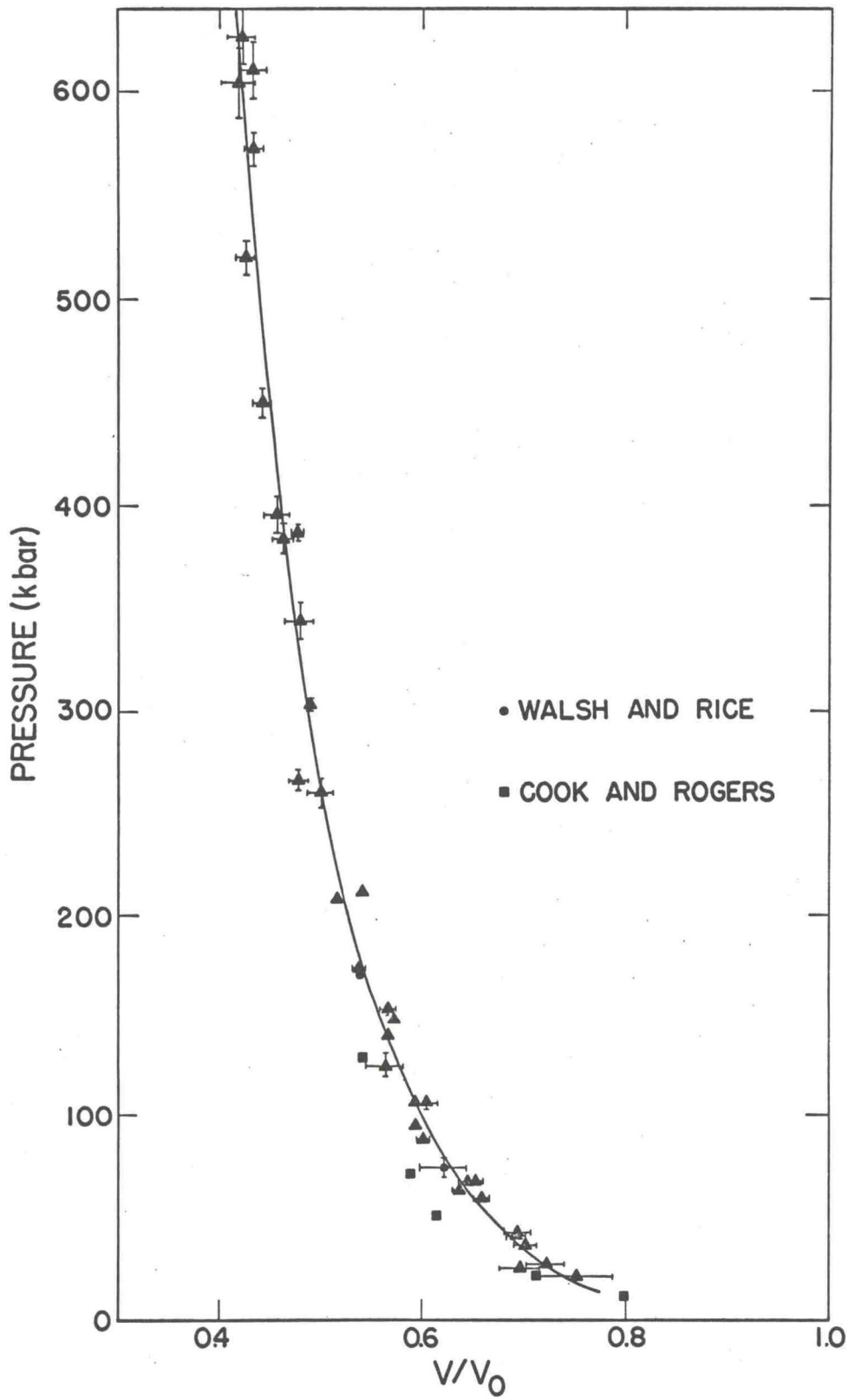

Fig. 21. Carbon tetrachloride pressure versus relative volume.

light beginning at about 70 kbar with complete opaqueness observed at approximately 150 kbar. It was concluded from this that the shock induced conductivity has a threshold pressure near 70 kbar. This has since been verified from work[44] conducted at the Lawrence Radiation Laboratory at Livermore. The break at 4.7 km/sec in the U_s-U_p plot corresponding to a pressure of nearly 150 kbar may have some significance to the observed high electrical conductivity and opaqueness of the shocked material at this pressure.

It is believed that the original carbon tetrachloride Hugoniot lies in a low temperature phase and then crosses the phase line into a high pressure and temperature phase. This explanation suggests the liquid form transforms to an ice or other solid form when crossing the phase line. Since the carbon tetrachloride molecule has spherical symmetry each molecule would need to rotate through only a relatively small angle to be oriented sufficiently for the formation of a solid structure. However, the Hugoniot temperature at the 150 kbar transition pressure is 2800°K and this high temperature may nullify this explanation.

G. Liquid Nitrogen

The Hugoniot data are presented in Table VIII and in Figs. 22 and 23. The Russian[17] data are plotted as solid circles. In the shock-particle velocity (U_s-U_p) plot, the points fit the straight line

$$U_s = 1.49 \pm 0.06 + 1.49 \pm 0.02 U_p$$

up to a shock velocity of about 7.4 km/sec. Above this velocity the behavior is not well established and prevents relating the individual

Table VIII. Shock wave data for the liquid nitrogen Hugoniot.

Shot No.	Initial density (g/cc)	Shock vel.[a] (km/sec)	Particle vel. (km/sec)	Pressure (kbar)	Relative vol. V/V_0
1	0.820	2.58 ± 0.02	0.75 ± 0.10	16.0 ± 2.0	0.708 ± 0.037
2	0.820	2.97 ± 0.02	0.97 ± 0.05	23.6 ± 1.2	0.674 ± 0.016
3	0.820	3.53 ± 0.01	1.39 ± 0.04	40.1 ± 1.0	0.606 ±0.010
4	0.820	4.19 ± 0.02	1.85 ± 0.03	63.5 ± 1.1	0.558 ± 0.008
5	0.820	5.09 ± 0.02	2.44 ± 0.02	102 ± 1	0.521 ± 0.004
6	0.820	5.50 ± 0.02	2.69 ± 0.02	121 ± 1	0.512 ± 0.005
7	0.820	5.92 ± 0.03	2.90 ± 0.12	141 ± 6	0.510 ± 0.021
8	0.820	6.66 ± 0.03	3.54 ± 0.07	193 ± 4	0.469 ± 0.010
9	0.820	6.98 ± 0.08	3.64 ± 0.09	208 ± 5	0.479 ± 0.014
10	0.820	7.34 ± 0.04	3.98 ± 0.08	239 ± 5	0.458 ± 0.011
11	0.820	7.52 ± 0.05	4.26 ± 0.07	263 ± 5	0.434 ± 0.010
12	0.820	7.59 ± 0.03	4.32 ± 0.12	269 ± 8	0.431 ± 0.016
13	0.820	7.43 ± 0.03	4.38 ± 0.08	267 ± 5	0.410 ± 0.011

Table VIII. (continued)

Shot No.	Initial density (g/cc)	Shock vel.[a] (km/sec)	Particle vel. (km/sec)	Pressure (kbar)	Relative vol. V/V_0
14	0.820	7.73 ± 0.03	4.50 ± 0.10	285 ± 6	0.418 ± 0.013
15	0.820	8.17 ± 0.06	4.55 ± 0.09	305 ± 6	0.443 ± 0.012
16	0.820	7.92 ± 0.05	4.60 ± 0.11	299 ± 7	0.420 ± 0.014
17	0.820	8.36 ± 0.06	4.69 ± 0.08	321 ± 6	0.440 ± 0.011
18	0.820	8.51 ± 0.08	4.86 ± 0.05	339 ± 4	0.429 ± 0.008
19	0.820	8.48 ± 0.03	5.04 ± 0.11	350 ± 8	0.406 ± 0.013
20	0.820	8.82 ± 0.04	5.20 ± 0.10	376 ± 7	0.411 ± 0.011
21	0.820	8.92 ± 0.06	5.30 ± 0.12	388 ± 9	0.406 ± 0.015

[a]The shock velocity listed reflects a 0.2% reduction of the value measured from the raw time-distance data due to thermal contraction.

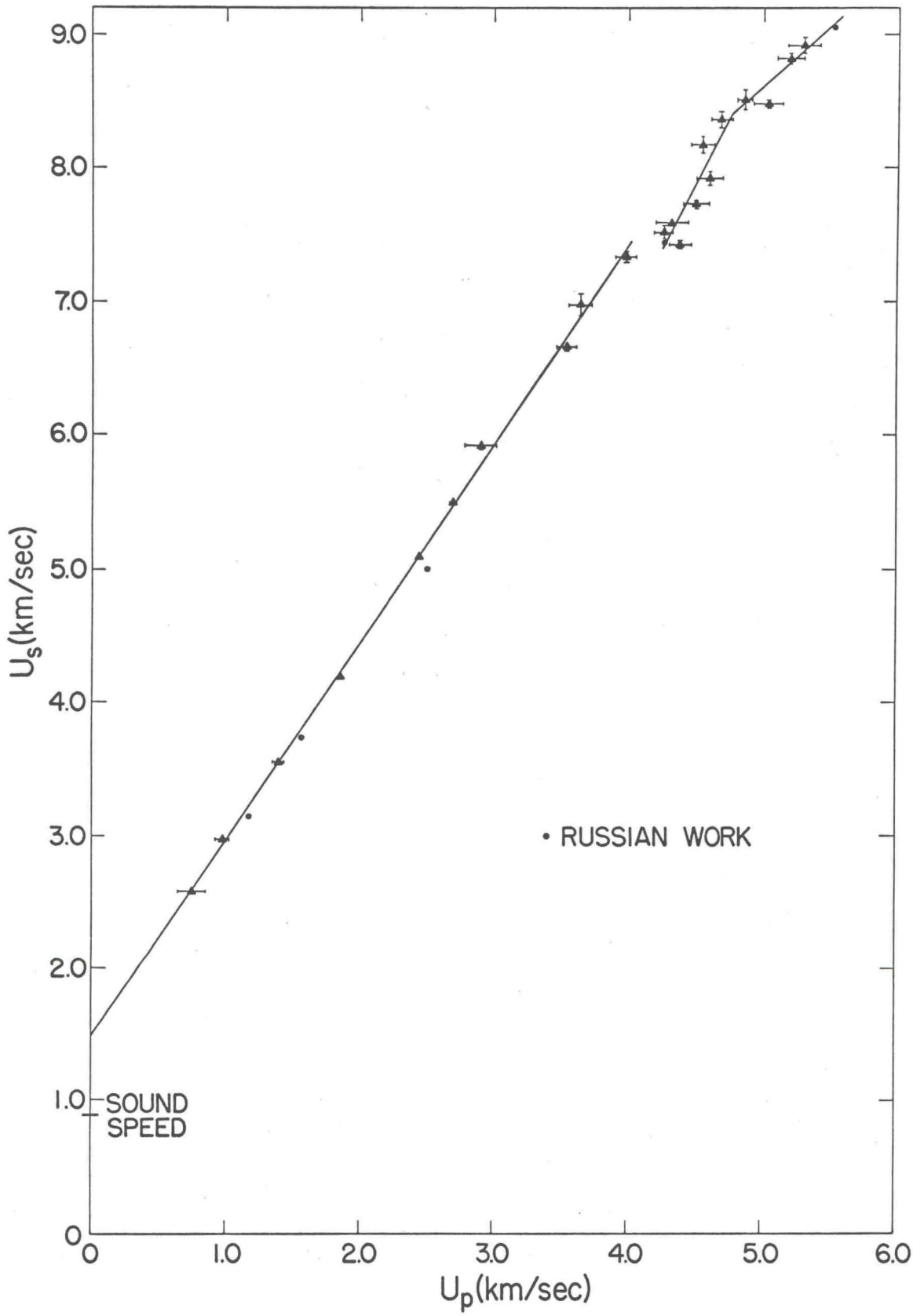

Fig. 22. Liquid nitrogen shock velocity versus particle velocity.

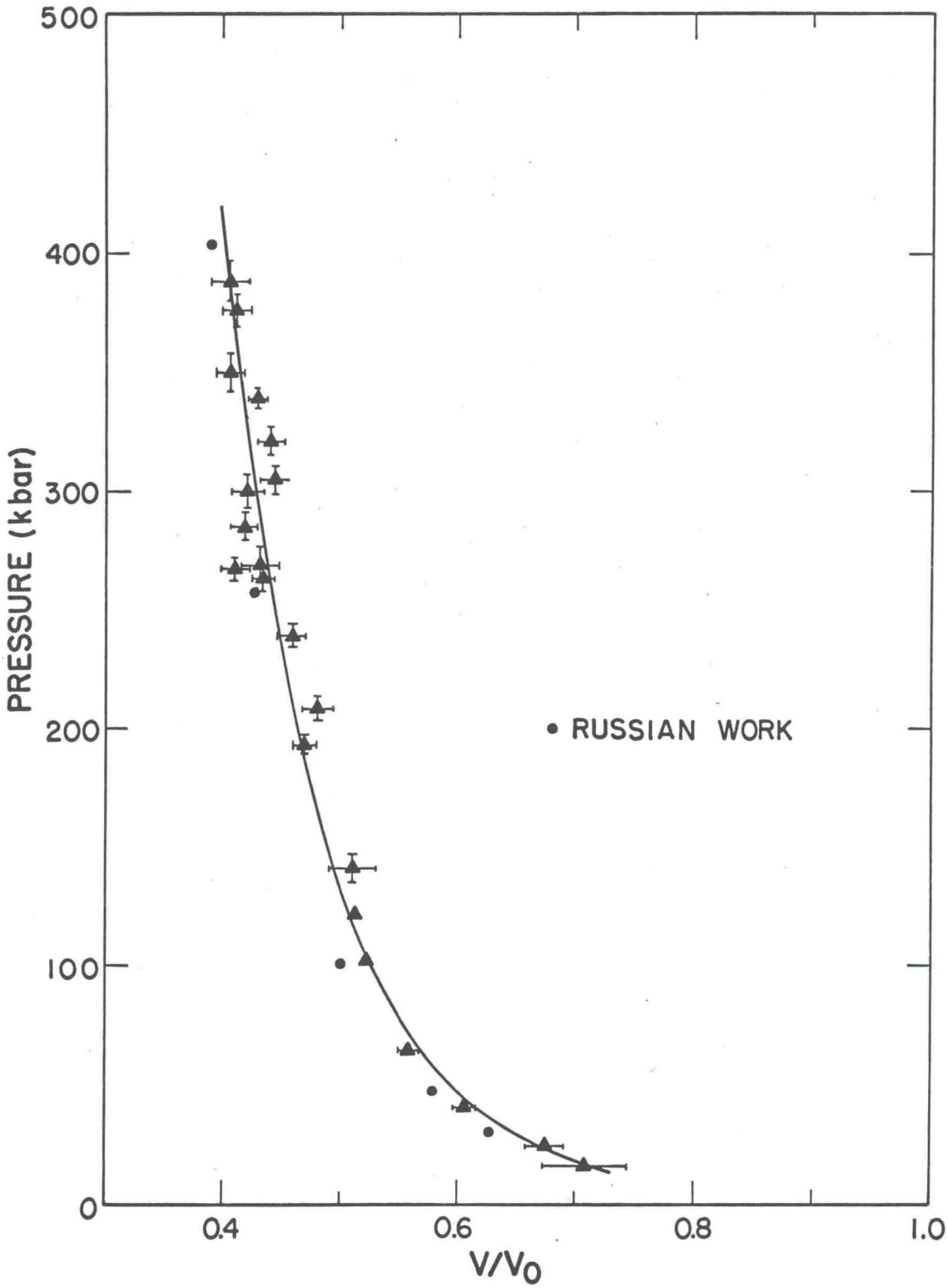

Fig. 23. Liquid nitrogen pressure versus relative volume.

points in a straightforward manner. An interpretation that fits all the upper data except for one point is suggested by two lines in this region. Region 2 for the shock velocity range of 7.4 to 8.4 km/sec is described by

$$U_s = -1.0 \pm 2.0 + 2.0 \pm 0.4 U_p.$$

The data of region 3 which extends from 8.4 to 9.0 km/sec fits the equation

$$U_s = 4.06 \pm 0.05 + 0.92 \pm 0.01 U_p.$$

It is not known at the present time whether this behavior is real or a manifestation of some undiscovered systematic experimental error.

The Russian data agree fairly well with the present data at the lower end. Their two highest points bracket the disordered region and consequently provide no help in clarifying the situation. Their experimental techniques were very similar to those used here in that the shock velocity is measured by the electrical pin technique and then impedance matched to an aluminum standard.

Another observation gained from the U_s-U_p plot is that the fitted line extrapolates to a velocity on the U_s axis which is higher by about 70% than the reported sound speed[45] of 0.88 km/sec. Freezing may take place under dynamic conditions below pressures of 16 kbar. Bridgman[13] has reported melting data for nitrogen to nearly 6 kbar.

No two-shock wave experiments were conducted; primarily because at these low temperatures the required experimental apparatus make the experiments very difficult. In addition, no electrical conductivity experiments were performed, but might prove interesting.

All the liquid nitrogen pressure-relative volume ($P\text{-}V/V_0$) Hugoniot data in Fig. 23 were fit to a single concave upward curve. Due to inadequate precision, the $P\text{-}V/V_0$ curve does not reflect the observed breaks in the lines which characterize the $U_s\text{-}U_p$ data. The curve is expressed by

$$P = 16V/V_0 + 7(V/V_0)^2 + 111(V/V_0)^3.$$

When comparing the two sources of data, the general impression is that the present data indicates a stiffer material than does the Russian data. Since the Russian's starting point was 77°K and a density of 0.808 g/cc instead of 75°K and a density of 0.820 g/cc for the present data, some of the observed deviation may originate from these differences. Also, it is not clear from the Russian paper whether the aluminum standard was pure aluminum or an alloy. If the standards were not identical this would contribute to the difference in the two Hugoniot curves.

The $U_s\text{-}U_p$ plot of several materials such as sodium chloride[46] and bismuth[28] are similar to that of liquid nitrogen. A possible phase system[28] which could produce the observed $U_s\text{-}U_p$ diagram is presented in Fig. 24. The Hugoniot is hypothesized to pass through three phases near a triple point. For the liquid nitrogen case, the Hugoniot starts out in the liquid phase and crosses into phase I at a pressure of 240 kbar. Then the Hugoniot crosses into phase II at a pressure of 330 kbar. The temperature associated with the 240 kbar Hugoniot pressure is about 7200°K and is even higher for 330 kbar. Hence the two phases may be atomic nitrogen ordered in some compact form.

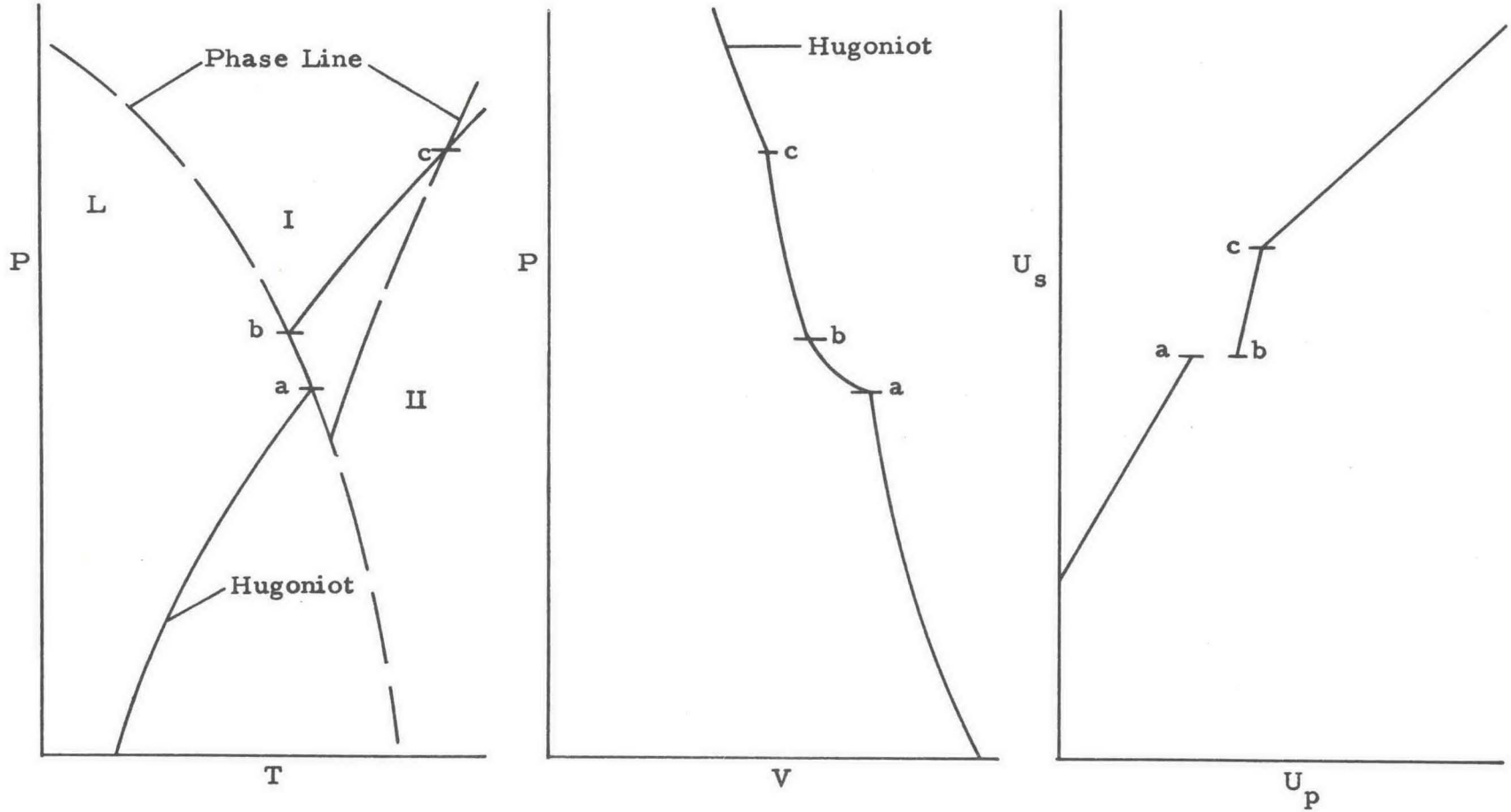

Fig. 24. Hugoniot passing through three phases.

H. Some Thermodynamic Calculations

The results of some thermodynamic calculations made with the computer program described briefly in Section C of this chapter are presented to illustrate the type of information obtained. Benzene was chosen as representative of the behavior for all the liquids with respect to isotherms and isentropes. Fig. 25 is a graph of an isotherm and an isentrope centered at 125 kbar on the Hugoniot, an isentrope centered at zero pressure, and the Hugoniot curve. No calculations were made above the transition pressure because of the lack of knowledge of the high pressure phase. As illustrated, the pressure on the isotherm is slightly less than the pressure on the isentrope for a given volume when to the left of the Hugoniot. The reverse is the case when to the right of the Hugoniot. The two isocurves are very close together and also are not separated much from the Hugoniot curve.

Some other calculated results at the transition point are listed in Table IX. The values for the sound speed and temperature seem reasonable except the temperature calculated for liquid nitrogen using the $C_p(T)$ data in Table IV is seemingly too high. A temperature of 700°K is calculated when using the classical specific heat value of 5/2R for a diatomic molecule (R is the universal gas constant) which is probably much too low. An inadequate model for the equation of state along with insufficient initial data is blamed for the uncertainty.

One of the listed values is the best fit gamma (Γ_f). It represents a value for the Gruneisen gamma which best fits the

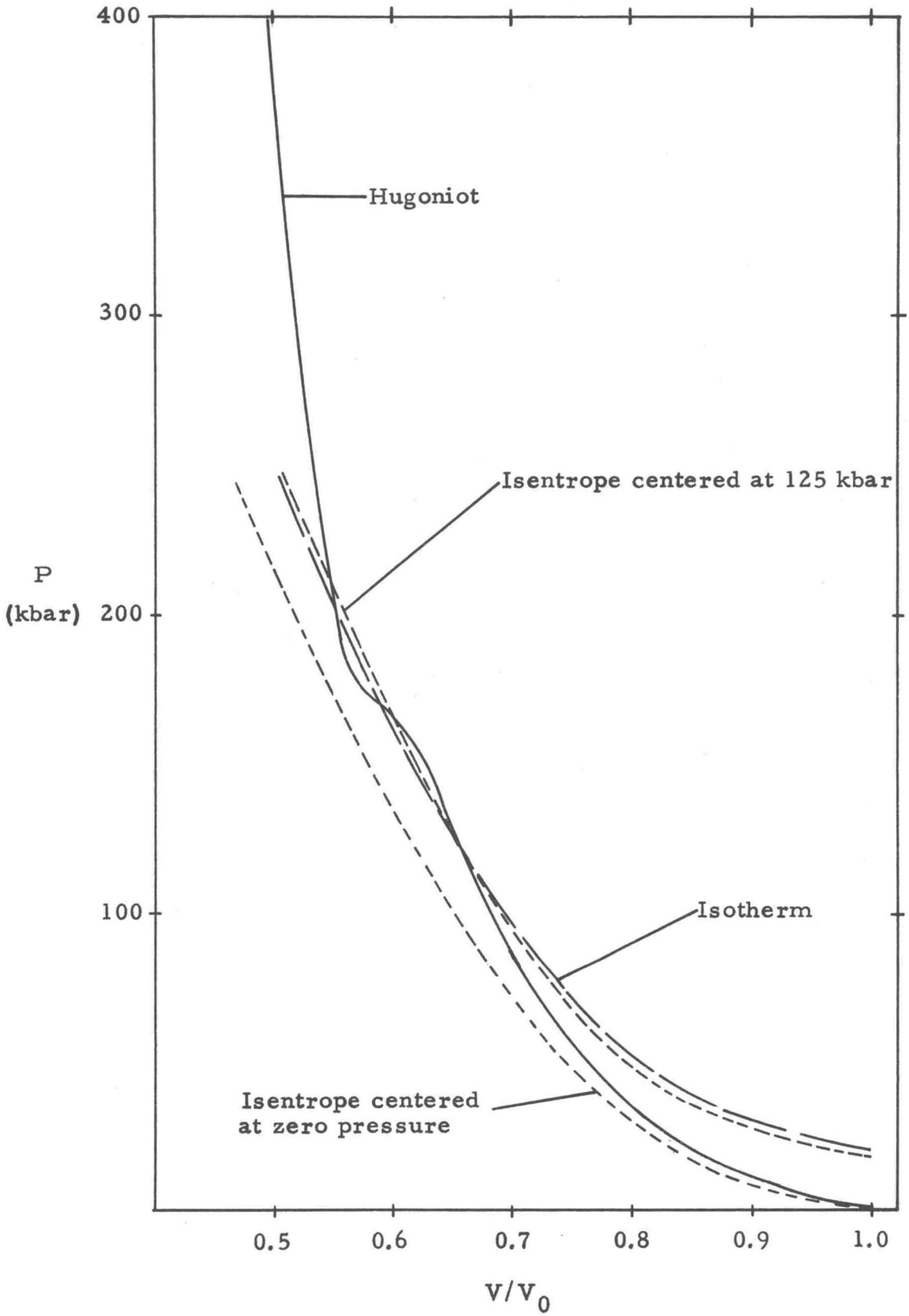

Fig. 25. Benzene isentrope, isotherm, and Hugoniot.

Table IX. Some calculated thermodynamic quantities and pertinent experimental data.

	Benzene	Carbon disulfide	Carbon tetrachloride	Liquid nitrogen
Lower U_s-U_p slope	1.58	1.46	1.57	1.49
Middle U_s-U_p slope	0.43	---	---	2.00
Upper U_s-U_p slope	1.34	1.32	1.31	0.90
Transition pressure (kbar)	125	64	150	240
Hugoniot temperature at transition (K)	2200	1000	2800	7200
Sound speed on Hugoniot at transition (km/sec)	7.2	3.8	5.3	7.1
Best fit gamma (Γ_f)	2.39	1.86	3.10	4.20
Thermodynamic gamma (Γ_0)	1.20	1.56	1.25	2.24
Hugoniot energy at transition (erg(10^{10}))	3.9	1.0	2.0	7.9

experimental data and is to be compared to the thermodynamic gamma (Γ_0) calculated from initial data using Eq. (29). The best fit gamma is the value obtained from Γ/V constant at $V = V_0$. The value for Γ_f is computer determined from a program written by John Skalyo, Jr. In the code, a Mie-Gruneisen form of the equation of state is assumed along with the approximation that Γ/V is constant as stated in Eq. (30). The mathematical development is similar to Section F of Chapter II. Essentially the program minimizes the energy on an isentrope and the enthalpy at zero compression with respect to Γ/V = constant. The range of Hugoniot starting pressures for the isentropes is chosen so that at zero compression the region of validity for the specific heat and volume expansion data is not exceeded. As can be seen from Table IX, the best fit gamma and the thermodynamic gamma compare poorly. This is due in part to the inadequate zero-pressure initial data which provides only a small pressure range over which the energies can be minimized. It is also believed that the Mie-Gruneisen model is not suitable for liquids. Instead of assuming Γ/V is constant it may be necessary to include volume dependant terms of the form

$$\Gamma/V = \Gamma_0/V_0 + F(V)$$

where Γ_0/V_0 is the thermodynamic value and $F(V)$ is some function of volume, possibly a series expansion. This hypothesis remains to be investigated.

V. SUMMARY

A. Present Investigation

The investigation of these four liquids revealed several features common to all. First, all the liquids exhibit a linear relationship of the form $U_s = C + MU_p$ between the shock velocity and the particle velocity with the possible exception of carbon tetrachloride. Based on this observation, it is hypothesized that most liquids can be described in terms of the linear relationship between the two velocities. Secondly, all the liquids were observed to undergo some type of transition with benzene, carbon disulfide, and liquid nitrogen yielding the largest volume change. The nature of the high pressure phase for these three liquids is probably very much different from the original liquid state. Freezing could fit the observed behavior for carbon tetrachloride. Thirdly, the intercept of the lower U_s-U_p line with the U_s axis is at a higher value than the measured sound speeds. This could signify a transition occurring below the pressures accessible by the techniques employed in this study. Fourth, carbon disulfide and carbon tetrachloride both exhibited a very large increase in electrical conductivity with pressure while benzene did not for pressures up to 140 kbar. Other similarities are available from the data listed in Table IX.

The experimental apparatus for the organic liquids is basically sound, relatively easy to fabricate, and provides space to

shock three liquids at a time. There are, however, some changes which could improve the precision of the velocity measurements. They are (1) to provide better control of the temperature and density of the liquids so that the initial and final states lie on the same Hugoniot for each shot, (2) to use a standard target material which has an impedance closer to the liquid samples than 2024 dural, (3) to use higher purity liquids, and (4) to require closer tolerances on the parallelism and flatness of the explosive charges and target plates and the setback between the center electrode and silver cap in the coaxial pins. This last suggestion would increase the cost and time necessary to construct the experimental apparatus, however.

The results of the liquid nitrogen study indicate that shock Hugoniot data at these low temperatures can be obtained. The present design, however, needs to be investigated in the light of the poorer liquid nitrogen data obtained at high pressures. In order to study other materials at low temperatures, the apparatus needs some modification. The design was modified in a study of solid argon[47] at 75°K with good results. The precision could be improved if the Hugoniot for the standard target material were known and the pin depths and setbacks were actually measured at liquid nitrogen temperatures. Some of the improvements mentioned above for the organic liquids could also be adopted.

B. Future Studies

It would be desirable to obtain more data on benzene in the neighborhood of the transition to provide a better basis for interpretation. This may prove difficult since the material at this pressure

is in a mixed phase condition and would not yield accurate data for either phase. As mentioned previously, the pressure region above 240 kbar for liquid nitrogen needs to be investigated further to determine conclusively if a transition occurs or is an experimental artifice. Higher pressure data for all the liquids would add to the knowledge of the Hugoniots already obtained.

Future experimentation should include a thorough investigation of electrical conductivity as a function of pressure and temperature to provide a better opportunity for determining the nature of the transitions and the transformed materials. In addition, identifying the type of electrical conductivity may aid in determining the nature of the compressed materials.

Another technique which could prove useful is the recovery of shocked samples for further analysis. Unless the experiment is properly designed, the presence of rarefaction waves, interactions, and multiple shocks may obscure the results sufficiently to render an interpretation questionable.

Some interesting liquids and solids for further study would be the condensed noble gases such as helium, neon, kypton, and others. The data from them is more adaptable to theoretical analysis because the atoms do not bond together to form a molecule in the different phases. Also, the experiments could be conducted to stay within the framework of the Law of Corresponding States providing a basis for comparison on theoretical grounds.

Other interesting liquids would be n-hexane and cyclohexane. The Hugoniot for cyclohexane, whose molecule is six CH_2 groups arranged in a benzene ring, and n-hexane, whose molecule

consists of four CH_2 groups arranged linearly with a CH_3 group at each end, could be compared with each other and with the benzene Hugoniot. The purpose of this comparison would be to learn the effects molecular structure and the additional hydrogen atoms have on the characteristics of the Hugoniot curves, transition pressures, and electrical properties.

There is also the series of Freons in the liquid and solid forms for which the Hugoniots could be compared in the search for a systematic behavior. Also, a study of the substituted methanes which includes carbon tetrachloride remains to be done in the liquid and solid forms. The number of interesting substances that could be investigated by dynamic methods is practically unlimited and the problem is to sort out those that would yield the most useful high pressure information amenable to theoretical interpretation.

REFERENCES

[1] J. Canton, Phil. Trans. Roy. Soc., 640(1762).

[2] J. Perkins, Trans. Roy. Soc., 324(1819).

[3] L. Cailletet, Compt. Rend. 75, 1131(1872).

[4] E.H. Amagat, Ann. Chim. Phys. 29, 68(1893).

[5] G. Tammann, Z.S. Phys. Chem. 11, 676(1893).

[6] T.W. Richards, Pub. Carnegie Inst. Wash. No. 7, (1903).

[7] P.W. Bridgman, Proc. Am. Acad. Arts Sci. 49, 3(1913).

[8] P.W. Bridgman, Proc. Am. Acad. Arts Sci. 66, 185(1931).

[9] P.W. Bridgman, J. Chem. Phys. 9, 794(1941).

[10] P.W. Bridgman, Proc. Am. Acad. Arts Sci. 74, 399(1942).

[11] P.W. Bridgman, Proc. Am. Acad. Arts Sci. 77, 129 (1949).

[12] P.W. Bridgman, Phys. Rev. 46, 930(1934).

[13] P.W. Bridgman, Proc. Am. Acad. Arts Sci. 70, 1(1935).

[14] J.M. Walsh and M.H. Rice, J. Chem. Phys. 26, 815(1957).

[15] M.H. Rice and J.M. Walsh, J. Chem. Phys. 26, 824(1957).

[16] M.A. Cook and L.A. Rogers, J. Appl. Phys. 34, 2330(1963).

[17] V.N. Zurborev and G.S. Telegin, Soviet Phys.-Doklady 7, 349(1963).

[18] M. van Thiel and B.J. Alder, J. Chem.Phys. 44, 1056(1966).

[19]R. Courant and K.O. Friedrichs, Supersonic Flow and Shock Waves (Interscience Publishers, Inc., New York, 1948), Chap. III, pp. 141-146.

[20]L.D. Landau and E.M. Lifschitz, Fluid Mechanics (Addison-Wesley Publishing Co., Inc., Reading, Mass., 1959), Chap. 9.

[21]M.H. Rice, J.M. Walsh, and R.G. McQueen, Solid State Physics Academic Press Inc., New York, 1958), Vol. 6, pp. 1-63.

[22]W.E. Deal, Jr., Modern Very High Pressure Techniques edited by R.H. Wentorf (Butterworths, Washington, 1962), Chap. 11.

[23]G.E. Duval and G.R. Fowler, High Pressure Physics and Chemistry (Academic Press Inc., New York, 1963), Vol. 2, Chap. 9.

[24]D. Bancroft, E.L. Peterson, and S. Minshall, J. Appl. Phys. 27, 291(1956).

[25]R.H. Warnes, J. Appl. Phys. 38, 4629(1967).

[26]R.G. McQueen and S.P. Marsh,(private communication)

[27]J.C. Slater, Introduction to Chemical Physics (McGraw-Hill Book Co., Inc., New York, 1939), Chap. XIII.

[28]R.G. McQueen, Metallurgy at High Pressures and High Temperatures, edited by K.A. Gschneidner, Jr., M.T. Hepworth, and N.D. Parlee (Gordon and Breach, New York, 1964), pp. 44-132.

[29]J. Berger and S. Joigneau, Compt. Rend. 249, 2506(1959).

[30]J.N. Fritz, (unpublished)

[31]M.W. Zemansky, Heat and Thermodynamics (McGraw-Hill Book Co., Inc., New York, 1957) 4th ed., p. 264.

[32]R.W. Goranson, D. Bancroft, B.L. Burton, T. Blecher E.E. Gittings, and S.A. Landeen, J. Appl. Phys. 26, 1472(1955).

[33]S. Minshall, J. Appl. Phys. 26, 463(1955).

[34]R.D. Dick and T.E. Gould, Rev. Sci. Instr. 36, 143(1965).

[35]R.G. McQueen and S.P. Marsh, J. Appl. Phys. 31, 1253(1960).

[36]M.A. Cook, R.T. Keyes, and W.O. Ursenbach, J. Appl. Phys. 33, 3413(1962).

[37]R.G. McQueen, S.P. Marsh, and J.N. Fritz, J. Geophysical Res. 72, 4999(1967).

[38]G.E. Duvall, Les Ondes de Detonation (Editions du Centre National de la Recherche Scientifique, Paris, 1962), pp. 337-352.

[39]H.G. Drickamer, Science 156, 1183(1967).

[40]E. Whalley, Can. J. Chem. 38, 2105(1960).

[41]E.G. Butcher, M. Alsop, J.A. Weston, and H.A. Gebbie, Nature 199, 756(1963).

[42]A.S. Kusubov, (private communication).

[43]R.D. Dick, Bull. Am. Phys. Soc. 9, 547(1964).

[44]R.N. Keeler and A.C. Mitchell, UCRL-14538, Progress Report, June-September 1965.

[45]A. Van Itterbeck and W. Van Dael, Physica 28, 861(1962).

[46]Unpublished sodium chloride data of Los Alamos Scientific Laboratory Groups GMX-4 and GMX-6.

[47]J. Skalyo, Jr., R.D. Dick, and R.H. Warnes, Bull. Am. Phys. Soc. (1968).